TÉCNICO LISBOA

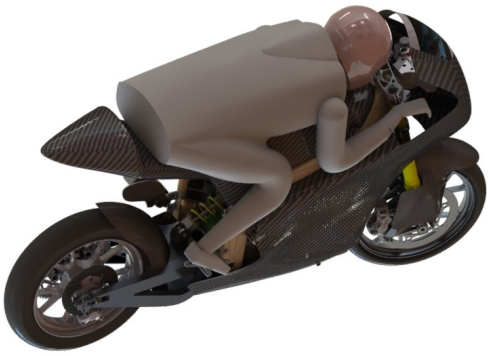

Motorcycle Modelling and Trajectory Controlling

Miguel Zambujo Orvalho

Thesis to obtain the Master of Science Degree in

Mechanical Engineering

Supervisor: Prof. Jorge Alberto Cadete Ambrósio

Examination Committee

Chairperson: Prof. Paulo Rui Alves Fernandes
Supervisor: Prof. Jorge Alberto Cadete Ambrósio
Member of the Committee: Prof. Luís Alberto Gonçalves de Sousa

October 2021

Acknowledgments

Começo por apresentar a minha gratidão ao meu orientador, Professor Jorge Ambrósio, por todo o seu compromisso e disponibilidade durante toda a realização deste trabalho. O seu entusiasmo e apoio foram imprescindíveis para manter o foco e alcançar a motivação necessária.

A todos os meus colegas da equipa TLMoto, por todas as experiências vividas e conhecimento partilhado ao longo dos últimos tempos. Com eles, intensificou-se o meu gosto pelo motociclismo.

Não poderia esquecer de agradecer aos meus amigos pelas horas de trabalho partilhadas, as pausas emotivas e os conselhos dados.

Um agradecimento muito especial à minha namorada, que no cumprimento dos seus objectivos ajudou-me a alcançar os meus. Onde o tempo dedicado a este trabalho, não poderia ter sido passado de melhor forma.

Por último, agradeço à minha família pelo apoio incondicional. Sempre me disseram para fazer o que mais gostasse e que lutasse por isso. Tentaram sempre proporcionar-me o melhor caminho e experiências enriquecedoras. Com todo este incrível apoio, apresento este trabalho.

Resumo

O conhecimento do comportamento dinâmico de um motociclo, permite o seu desenvolvimento e melhoria de performance, principalmente a nível da competição. No presente trabalho, é discutido o comportamento dinâmico de um motociclo, referindo condições limites em diferentes cenários, e realçados alguns aspectos dinâmicos referentes ao movimento da direção. É apresentada a formulação necessária à construção de um modelo multicorpo de um motociclo, onde é ainda implementado um ”driver” cinemático, para o controlo da direção. São discutidas as principais forças externas envolvidas num veículo de estrada e abordados alguns dos modelos de pneu mais usados na descrição das forças envolvidas no contacto entre o pneu e a estrada.

A detecção de contacto entre o pneu e a estrada é formulada, abordando os aspectos do contacto entre uma estrada não plana, com a geometria típica de um pneu de motociclo. São discriminadas as expressões das quantidades cinemáticas necessárias à implementação do modelo de pneu *Pajecka Magic Formula*, onde a sua implementação é comparada com a literatura. Sendo as forças de contacto desenvolvidas num ponto de contacto do pneu, é apresentado ainda a transferência dessas mesmas forças para o corpo roda.

O modelo multicorpo, composto por corpos rígidos e elementos de suspensão, é baseado no protótipo elétrico TLM03e desenvolvido pela equipa TLMoto do IST. Revestidas as rodas do modelo do motociclo com o modelo de pneu apresentado, o modelo do motociclo é testado no cenário simples em linha recta.

O controlo do motociclo é apresentado através da implementação de um controlador LQR, onde são derivadas as equações simplificadas para o equilíbrio do motociclo. É sugerido um modelo reduzido, para controlo da mota em diferentes cenários, e discutida a ideia do seguimento de uma linha de referência através do ângulo de inclinação do motociclo.

Palavras-chave: Dinâmica multicorpo, Dinâmica de motociclo, Pacejka Magic Formula, Controlo de motociclo, Motociclo de competição

Abstract

The knowledge of the dynamic behaviour of a motorcycle allows its development and performance improvement, mainly at the level of competition. In the present work, the dynamic behaviour of a motorcycle is discussed, referring to limit conditions in different scenarios, and some dynamic aspects related to the steering movement are highlighted. The formulation necessary for the construction of a multibody model of a motorcycle is presented, where a kinematic ”driver” for steering control is also implemented. The main external forces involved in a road vehicle are discussed and it is approached some of the most used tire models in describing the forces involved in the contact between the tire and the road.

The detection of contact between the tire and the road is formulated, addressing the aspects of the contact between a non-flat road, with the typical geometry of a motorcycle tire. The expressions of the kinematic quantities necessary for the implementation of the tire model *Pajecka Magic Formula* are discriminated, where its implementation is compared with the literature. Being the contact forces developed at a tire contact point, the transfer of these forces to the wheel body is also shown.

The multibody model, consisting of rigid bodies and suspension elements, is based on the TLM03e electric prototype developed by the TLMoto team in IST. With the wheels of the motorcycle model coated with the tire model presented, the motorcycle model is tested in the simple straight-line scenario.

The control of the motorcycle is presented through the implementation of an LQR controller, where the simplified equations for motorcycle equilibrium are derived. A reduced model is suggested, for controlling the motorcycle in different scenarios, and it is discussed the idea of following a reference line through the motorcycle’s roll angle.

Keywords: Multibody Dynamics, Motorcycle Dynamics, Pacejka Magic Formula, Motorcycle Control, Racing Motorcycle

Contents

List of Tables

List of Figures

List of Symbols

Convection

a, A, α	Scalar
$\mathbf{a}$	Vector
$\mathbf{A}$	Matrix

Overscript

$\dot{\mathbf{a}}$	First time derivative
$\ddot{\mathbf{a}}$	Second time derivative
$\tilde{\mathbf{a}}$	Skew-symmetric matrix, used to define the vector product

Superscript

$\mathbf{a}'$	Vector defined in a local reference frame
$\mathbf{a}^{\mathbf{P}}$	Vector associated with point P
$\mathbf{a}^{\mathbf{T}}$, $\mathbf{A}^{\mathbf{T}}$	Vector or matrix transpose

Subscript

$\mathbf{a}_i$	Referred to body i
$\mathbf{a}_j$	Referred to body j
$\mathbf{a}_r$	Referred to road
$\mathbf{a}_w$	Referred to body wheel
a_f	Quantity associated to the front of the motorcycle
a_r	Quantity associated to the rear of the motorcycle
a_M	Quantity associated to the motorcycle

Latin Symbols

$\ddot{\mathbf{x}}$	Motorcycle acceleration

$\mathbf{A}$	Transformation matrix
$\mathbf{B}$	Control input matrix
$\mathbf{C}$	Control system matrix
$\mathbf{f}$	Generic force vector
$\mathbf{f}_D$	Drag force
$\mathbf{f}_f$	Braking force actuated on the front wheel
$\mathbf{f}_r$	Braking force actuated on the rear wheel
$\mathbf{f}_y$	Lateral force actuated on the motorcycle
$\mathbf{g}$	Gravity vector; force vector on multibody analysis
$\mathbf{K}_{FB}$	Feedback optimal gain matrix
$\mathbf{M}$	Mass matrix
$\mathbf{m}$	Generic moment vector
$\mathbf{N}$	Control input matrix
$\mathbf{n}_f$	Normal force actuated on the front wheel
$\mathbf{n}_r$	Normal force actuated on the rear wheel
$\mathbf{n}_{sr}$	Static load actuated on the rear wheel
$\mathbf{n}_{tr}$	Transfer load
$\mathbf{p}$	Euler parameters vector
$\mathbf{Q}$	Weighting matrix
$\mathbf{q}, \dot{\mathbf{q}}, \ddot{\mathbf{q}}$	Vectors of generalized coordinate, velocities and accelerations
$\mathbf{R}$	Weighting matrix
$\mathbf{r}$	Position vector
$\mathbf{s}$	Driving force; Position vector of a point with respect to the fixed body frame
$\mathbf{u}$	Control vector
$\mathbf{z}, \dot{\mathbf{z}}$	State vector and its time derivative
a	Trail
b	Distance from Motorcycle CoG to rear wheel axis
c	Damping constant

C_z	Radial stiffness coefficient
d	Forward offset
D_z	Radial damping coefficient
e_0, e_1, e_2, e_3	Euler parameters
F_{z0}	Wheel nominal force
h	Height of the motorcycle CoG
$I_{\xi\xi}, I_{\eta\eta}, I_{\zeta\zeta}$	Principal moments of inertia of a body
J	Performance index
k	Spring constant
l_0	Undeformed spring length
l_c	Segment length
L_{pre}	Distance preview
l_{pre}	Length preview
m	Motorcycle mass
p	Wheelbase
r_0	Wheel unloaded radius
R_2	Wheel carcass radius
R_3	Wheel toroidal radius
R_c	Radius of curvature
r_e	Wheel effective radius
R_f	Front wheel radius
R_r	Rear wheel radius
R_{pre}	Curvature preview
s_{pre}	Reference line length preview
s_t	Actual reference line length
T_{pre}	Time preview
V_{Cx}	Wheel longitudinal running velocity in point C
V_r	Wheel rolling velocity

V_{Sx}	Wheel longitudinal slip velocity in point S
V_{Sy}	Wheel lateral slip velocity in point S
V_x	Wheel forward velocity
X, Y, Z	Global coordinates

Greek Symbols

α	Slip angle
α^*	Lateral slip ratio
$\boldsymbol{\gamma}$	Vector of accelerations constraints equations
$\boldsymbol{\lambda}$	Vector of Lagrange multipliers
$\boldsymbol{\Omega}$	Angular velocity of the motorcycle
$\boldsymbol{\omega}$	Angular velocity of a body
$\boldsymbol{\Phi}$	Vector of kinematic position constraints
$\boldsymbol{\Phi}_q$	Jacobian matrix
$\delta, \dot{\delta}, \ddot{\delta}$	Position, velocity and acceleration of: steering angle; penetration depth
δ_f	Wheel steered angle
γ	Camber angle
κ	Longitudinal slip ratio
μ_p	Driving traction coefficient
Ω_r	Wheel rolling velocity
$\phi, \dot{\phi}, \ddot{\phi}$	Position, velocity and acceleration of roll angle
ϕ_M	Actual motorcycle roll angle
ϕ_{des}	Desired roll angle
τ	Rake angle
ξ, η, ζ	Body fixed reference frame

Acronyms

CAD	Computer Aided Design
CoG	Center of Gravity
ISO	International Organization for Standardization

Chapter 1

Introduction

1.1 Motivation

Multibody models are commonly used to represent a wide number of systems, mainly made of rigid or flexible components while exhibit large rotations and translation between them. They allow to simulating operation conditions without a complete physical prototype, saving resources.

In order to develop some of the system mechanical parts and characteristics, such as safety or performance, the use of control systems may be of importance. In the framework of motorcycle dynamics, control can be used to simulate a perfect rider in a track, in order to reach a performance goal or to reveal system limitations. It is also applicable on situations of overcome instant human control, such as in driverless condition, or to support the rider in specify trajectories.

The motorcycle model, in which the methods presented in this work are applied, is based on the TLM03e electric motorcycle prototype developed by TLMoto team in IST. The dynamic analysis of the model, not only allows understanding its response to different riding conditions but also reveals some aspects to improve. The implementation of a tire model and a controller, allows testing more developments of the motorcycle such as: suspension dynamics as a response on more realistic conditions and eventually leading to a motorcycle setup optimization.

With this purpose in mind, a virtual driver for the motorcycle is implemented to force it to follow a trajectory, while can be posteriorly improved. It is foreseen that the models and methods implemented in this work have a significant impact on the motorcycle development in a competition context.

1.2 Literature Overview

In this section, the topics of motorcycle dynamics are first reviewed focusing on different aspects such as general dynamics in tire mechanics of handling. The multibody formulation used to build and simulate the motorcycle model is done next. Finally, an overview on the motorcycle control and virtual driver is presented.

1.2.1 Motorcycle Dynamics

Vehicle dynamics play an important role in the engineering world as it is used daily for human mobility and the transportation of resources. With regard to motorcycles, they are increasingly used in the choice of short courses. Therefore, an understanding of the fundamental behaviour of motorcycles is required to reveal the mechanisms for control, and to highlight the conditions of instabilities that dangerously affect the rider's control capabilities. The dynamics of two-wheeled vehicles are very peculiar in contrast to other road vehicles. One of the aspects of the two-wheel system is that it is an unstable system by nature at low speeds. It has a range of velocities in which it is self-stable, where the necessary forces in the front wheel are developed to self-stabilize but, for higher velocities becomes unstable again [1].

Motorcycles, like other road vehicles, can be studied in three different cases: acceleration, braking and cornering. Each of these cases presents several limit conditions in terms of risk to safety or loss of performance, especially on motorcycles where the height of the center of mass is high compared to its wheelbase. Another aspect of two-wheeled vehicles is the non-intuitive movement of the steering to describe a curve [1, 2].

Suspensions are one of the fundamental aspects when it comes to stabilizing a motorcycle, increasing its performance and comfort. Different types of suspension systems have been developed for motorcycles, particularly for the rear suspensions. Many rear suspension configurations with different link geometries can be found [1, 2].

Largely associated with high competition, in addition to suspensions, is the geometry of the motorcycle and the behavior of the main components - frame and swingarm. The wide range of values that the motorcycle occupies with regard to the angle of inclination needed to turn, leads to the need to look at the frame and swingarm as non-rigid bodies. The stiffness values of these components are increasingly of utmost importance, especially when it comes to competition [2].

1.2.2 Multibody Dynamics

A typical approach to study a mechanical system is to defining it as a multibody system. A multibody system is composed by bodies or links, rigid or not, which the motion between each can be constrained by internal and external forces. The bodies are connected by kinematic joints, formulated by kinematic constraints equations [3]. In this work a revolute joint, a translational joint and a steering driver are presented. Forces elements are also present, regardless of being active or passive elements. In this work, a suspension element composed by a spring and a damper is presented, being this a passive force element. Among the various possibilities of external forces that can act on a system, in dynamic road vehicles, greater importance is given to the tire's contact with the ground. Many authors present different options for contact models [4, 5], but in order to portray the contact between tire and road, these stand out [6–8][9].

The main objective of the dynamic analysis, is to predict the motion of the system, knowing its initial conditions. Many commercial software accomplish that, but the program MUBODyn-Matlab, developed and created at IST, is the one used on this work. This allows to continue to improve the program, develop

some Add-ins and have more control about the work. The solution of the multibody equations of motion is obtained by integrating in time a set of Ordinary Differential Equations. Some stabilization are needed to not violate the constraint equations [10].

1.2.3 Tire Model

Since the contact between the tires and the ground is extremely important in dynamic vehicles, the attempt to reproduce it has been a subject of study over the years. It is a very complex subject, since the dynamic behavior of the tire depends on many factors, some of which are, for example: the conditions and geometry of the ground and the tire, and the kinematics and dynamics of the vehicle.

Being the motorcycle a road contact vehicle, it becomes important how this contact is described and how the forces between the ground and tire body are applied on the vehicle. An analytical tire model was proposed by [6–8], but more attention was payed to the semi-empirical tire model developed by [9], where a standard formula is used to calculate almost all forces developed in contact. Also in [9], in addition to the original tire model, a specific tire model for motorcycles was developed in order to meet the wide ranges of roll angle described by them. As it is a semi-empirical model, a large amount of experimental data, specific to each tire and dynamic conditions of use, is required.

Despite the complexity of the semi-empirical model, through the use of identification methods, a complete set of parameter values for contemporary tires can be derived [11]. The correct adjustment in the parameters makes it even possible to portray an asymmetric tire, being very relevant in high competition.

1.2.4 Motorcycle Controller

Some of the motorcycle accidents are not only human error but also bad motorcycle design. Also associated with external factors, such as wind or the condition of the ground, motorcycles are known to destabilize in two ways - weave and wobble instability effects [12]. One of the ways to study the appearance of these effects is to know the behavior of the motorcycle through a control system.

The development of control systems for motorcycles may address various objectives such as aids for driving or to implement virtual drivers. To this work the implementation of a virtual driver is the focus of the control system. The control strategy for motorcycles can be similar to cars as much as possible. A control methodology is presented in [13] for a car with four-wheel steering and application of traction and braking torques to each one of them. The strategy is later implemented in Matlab by [14] using a bicycle model.

As the motorcycle is a non-linear system, it becomes a challenge to use a linear model to control it. A state-feedback control such as linear quadratic control, is commonly used to control a motorcycle. In [15], both feedback and feedforward control are used to control a motorcycle by steering, by applying a torque on it. A similar approach is taken by [16], but an integral part to the feedback control is added.

There is no such thing as equations that exactly describe the dynamic behavior of a motorcycle. Therefore, one of the measures that can dictate a good control system, is the choice of state variables

and the simplified equations that describe the motorcycle dynamics. In [17] can be found the derivation of simplified equations of motion, where it is later applied to motorcycle by [15]. Other authors, such as [18], present a different derivation for the simplified equations for motorcycle equilibrium. A good guideline for the implementation of a LQR controller for motorcycles is found in [19], along with some explanation of the controller behaviour.

Describing a trajectory over a reference line is one of the great challenges faced by many authors on motorcycle control. A road preview is one of the strategies used, as it is similar to the way a human drives a vehicle [20].

1.3 Objectives

The main objective of this work is the development of a virtual driver for a racing prototype motorcycle, expressed by a multibody system, using a simplified linearized controller. In the process, it is described the implementation of an avant garde tire model and the comprehension of the contact between pneumatic tires and the ground. As last intention, the use of a reduced model to follow a reference line implicitly without adding the state variables of the reference line.

In Chapter 2, an overview regarding the dynamics of the motorcycle is presented. Three cases are approached - acceleration, braking and cornering - as well as the conditions limits for each of them. For Chapter 3, the multibody dynamics used to simulate the motorcycle dynamics is formulated. Here, is emphasized the necessity of formulate a steering driver. The Chapter 4 concentrates on the implementation of the tire model and the contact detection is described with detail. In Chapter 5, the motorcycle model is formulated and it is presented the first scenario in a straight line with an unassisted motorcycle. In Chapter 6, the reduced model is defined, among several possibilities, and the simplified equations for motorcycle equilibrium are derived. It is represented the implementation of the controller and the motorcycle is finally tested with control in some scenarios, where it is increased the difficult of control. Lastly, in Chapter 7, conclusions are presented together with recommendations for future work.

Chapter 2

Overview of Motorcycle Dynamics

Many people in the world of motor sports and beyond share a passion for motorcycles, being their peculiar dynamic behaviour one of the reasons for the attraction. Motorcycles are an unstable vehicle by nature, due to the fact that they must balance on two small contact areas with the ground. The geometric parameters of the vehicle have a great importance in motorcycle dynamics and stability, since they define the purpose of the motorcycle. Reference works, such as those by Cossalter [1] and Foale [2] present a detailed description of motorcycle dynamics, the influence of its geometry and of the many characteristic phenomenons associated to acceleration, braking, cornering and other dynamic characteristics and responses.

2.1 Motorcycle Geometry

Geometric parameters are used to characterize a motorcycle. Different sets of parameters lead to different dynamic behaviour, being those of the sport, off-road or touring motorcycles distinct from each other. Figure 2.1 shows some of the parameters more important to characterize a motorcycle.

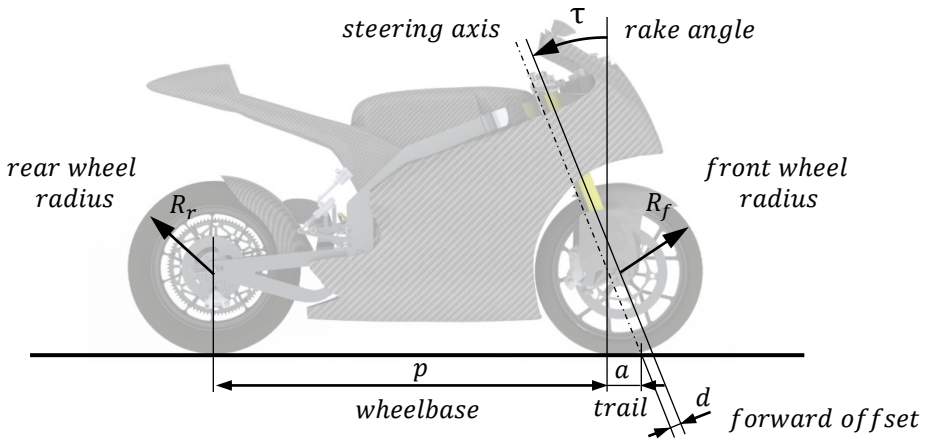

Figure 2.1: Geometric parameters that characterize a motorcycle.

Figure 2.1 shows the geometric parameters that characterized the motorcycle expected behaviour. These parameters can be associated with stability and maneuverability as depicted in Table 2.1. It should be noted that more stability means less maneuverability, being important to maintain an equilibrium between both in accordance to the purpose of the motorcycle.

Table 2.1: Relation between geometric parameters and motorcycle stability.

Geometric parameters	Stability
wheelbase, $p \uparrow$	$\uparrow$
rake angle, $\tau \uparrow$	$\uparrow$
trail, $a \uparrow$	$\uparrow$

A longer wheelbase stabilizes the motorcycle with respect to perturbations induced from road unevenness, but results in reduced maneuverability in cornering on curves with a small curvature radius. High values of trail, easily increased with the value of rake angle, contributes to increasing motorcycle steering stability, but makes steering harder. Lateral forces developed on the contact area of the front tire generates a higher aligning moment on the steering when trail increases. This means that the steering angle tends to be more easily restored to the steady position, making, in the forces, the steering of the motorcycle harder.

It is important to refer that motorcycle geometry change instantly when running, since they are composed by suspension elements whose relative positions can vary with the road geometry. The stiffness of motorcycle parts, mainly the frame and swingarm, also have a contribution to dynamics behaviour, being of extreme importance at higher velocities. The instability effects known as weave an wobble can occur on motorcycle [12], being the study of wobble effect important at higher velocities due to the flexibility of the main parts of a motorcycle. However, the flexibility of the motorcycle parts is not considered in the models developed in this work.

2.2 Rectilinear Motion

A rectilinear motion of a motorcycle can be seen as pure accelerating or braking scenarios. However, some limits for both cases are assumed considering steady state motion for simplicity. Figure 2.2 shows the angular motion around the common inertia axes, with origin on the center of mass of the motorcycle frame. This reference frame is used to describe motorcycle dynamics in general and the particular aspects of the virtual rider dynamics of this work, in particular.

The moments of inertia around the roll, pitch and yaw axis are some of the most relevant mass associated parameters for the motorcycle dynamics. The roll moment of inertia influences the ”resistance” of the motorcycle to the roll motion. Maintaining the center of gravity position, high values of roll moment of inertia slow down the entry and exit in a curve. Yaw moment of inertia influences the maneuverability as high values of yaw moment reduce the handling ability of the motorcycle. The pitch inertia, together with the wheelbase, have a strong influence on the motorcycle longitudinal dynamics, due to its ability to use both rear and front tires for braking/traction.

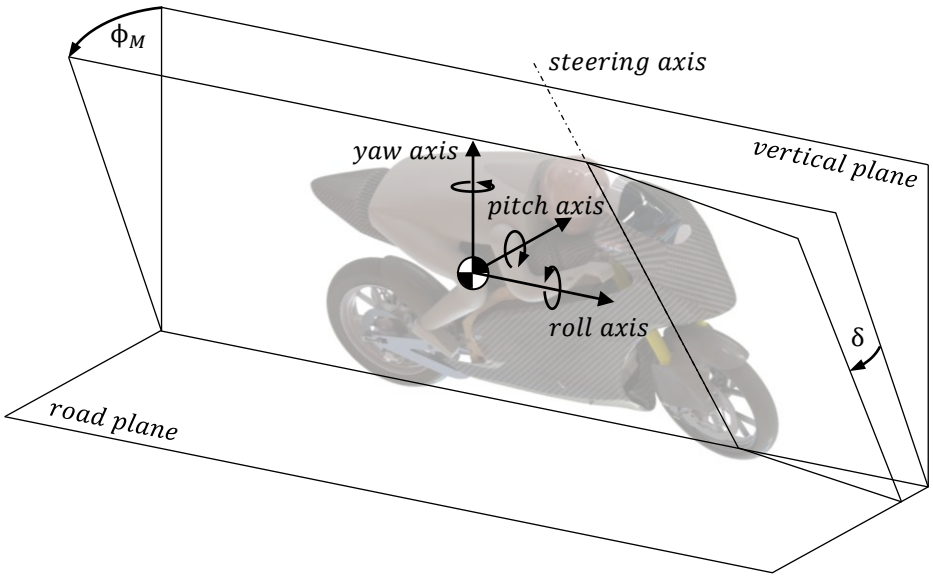

Figure 2.2: Definition of the inertia axis for the motorcycle dynamics. ϕ_M is the roll angle and δ the steering angle.

2.2.1 Acceleration

In the acceleration scenario, the motorcycle is subject to a driving force **s**, produced by the engine, on the rear wheel. **s** is given by $\mathbf{s} = m\ddot{\mathbf{x}} + \mathbf{f}_D$, where $\mathbf{f}_D$ is the drag force. Here the tire roll resistance moment is not considered. The driving force must be lower or equal to the product of the driving traction coefficient μ_p with the vertical load $\mathbf{n}_r$, getting $\mathbf{s} \leq \mu_p \mathbf{n}_r$, to avoid slippage.

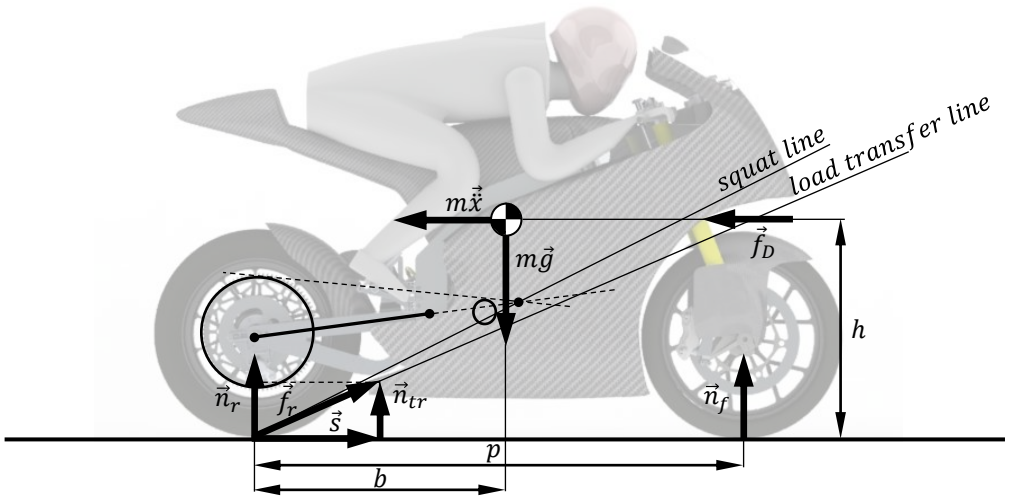

Figure 2.3: Motorcycle under acceleration (adapted from [1]).

One of the limit conditions in acceleration is the loss of traction on the rear wheel, meaning $\mathbf{s} > \mu_p \mathbf{n}_r$. This normally happens when motorcycle is at a lower speed and a large acceleration is produced. In competition a controller is used to avoid reaching the traction limit. The value of $\mathbf{n}_r$ and the maximum

acceleration, are written as:

$$\mathbf{n}_r = m\mathbf{g}\frac{(p-b)}{p} - \mathbf{s}\frac{h}{p} \tag{2.1}$$

$$\ddot{\mathbf{x}} \leq \frac{\mu_p \mathbf{g}\frac{p-b}{p}}{1-\mu_p\frac{h}{p}} - \frac{\mathbf{f}_D}{m} \tag{2.2}$$

where b is distance from motorcycle CoG to rear wheel axis.

Another limit condition in acceleration is the wheeling, which is achieved when there is no normal force on the front wheel. The following equations give $\mathbf{n}_f$ force condition and the maximum acceleration, respectively:

$$\mathbf{n}_f = m\mathbf{g}\frac{b}{p} - \mathbf{s}\frac{h}{p} = 0 \tag{2.3}$$

$$\ddot{\mathbf{x}} = \mathbf{g}\frac{b}{h} - \frac{\mathbf{f}_D}{m} \tag{2.4}$$

In acceleration, motorcycle squat motion has to be taken into account. The force $\mathbf{f}_r$ is given from the sum of $\mathbf{s}$ and the load transfer $\mathbf{n}_{tr}$. The vertical dynamic load is expressed as $\mathbf{n}_r = \mathbf{n}_{sr} + \mathbf{n}_{tr}$, where $\mathbf{n}_{sr}$ is the static load. Squat is the rearward pitching motion of the motorcycle. Squat motion is produced, depending on where the squat line and load transfer line are. If the load transfer line is under the squat line, it causes the extension of the rear spring. If the load transfer line is above the squat line, the rear spring is compressed, making the wheelie (negative rotation around the pitch axis) more likely to occur. Note that these lines vary all the time during a race.

2.2.2 Braking

In braking scenario, a braking force is produced by the brake system, aiming to reduce the velocity. A limit condition in braking is the forward flip over of the motorcycle, represented by the unloading of the rear wheel when the rear normal force becomes $\mathbf{n}_r = 0$.

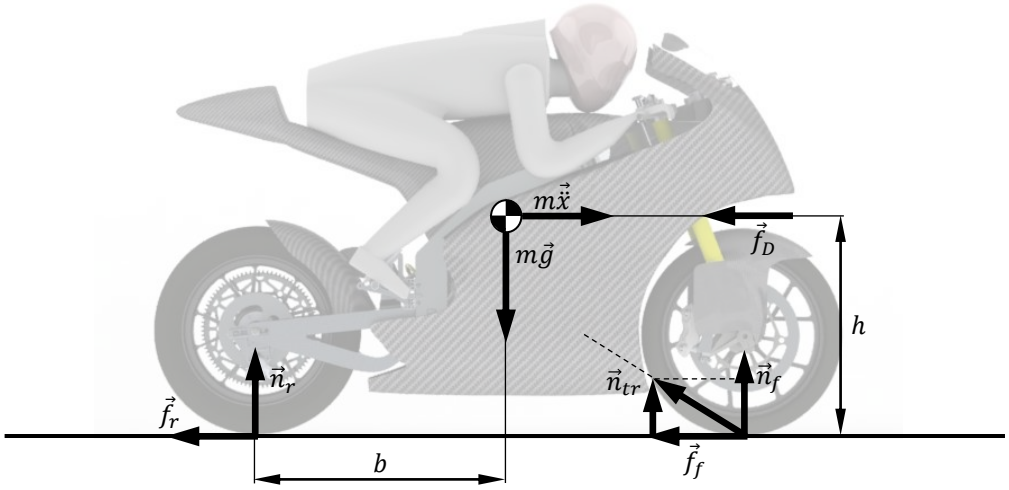

Figure 2.4: Motorcycle under braking (adapted from [1]).

Since $\mathbf{f}_r = 0$, the braking force is expressed as:

$$\mathbf{f}_f = \mathbf{n}_f \frac{p-b}{h} = m\mathbf{g}\frac{p-b}{h} \tag{2.5}$$

Taking into account the drag force $\mathbf{f}_D$, the maximum acceleration is limited by:

$$\frac{\ddot{\mathbf{x}}}{\mathbf{g}} \leq -\frac{p-b}{h} - \frac{\mathbf{f}_D}{m\mathbf{g}} \tag{2.6}$$

When braking, the motorcycle dive motion occurs, which is characterized by the forward pitching motion of the motorcycle. As expressed before, mass and center of mass position have an effect on dive. However, rake angle also has an important role on load transfer. When the direction of the resultant of the forces $\mathbf{n}_{tr}$ and $\mathbf{f}_f$ has the same angle, with respect to the normal to the road, as rake angle, the dive motion is more accentuated.

2.3 Cornering

In a cornering scenario, a motorcycle has to lean to compensate the centrifugal forces due to the curving of the motorcycle. Considering steady state motion and neglecting some of the gyroscopic effects, a motorcycle in cornering can be understood in plane, simply by the force equilibrium between the centrifugal and gravity forces as shown on the Figure 2.5, i.e., the direction of the resultant must intersect the line on the road between the two contact patches of the tire. The rolling resistance moment associated to the leaning of the motorcycle is disregarded in this equilibrium of forces.

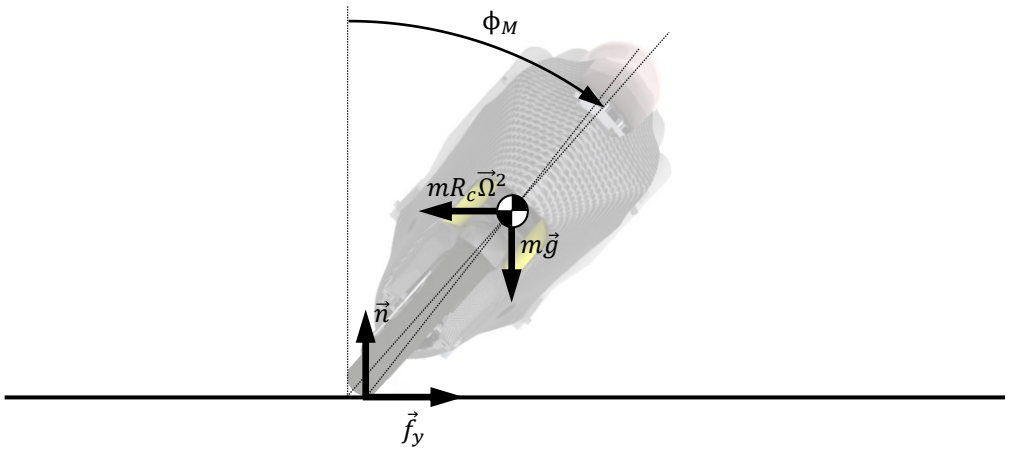

Figure 2.5: Motorcycle under cornering (adapted from [1]).

Instantaneously, for a given velocity, roll and steering angle of the motorcycle in steady state curving, there is an associated trajectory. The steering behaviour depends on the geometric parameters of the motorcycle, some of them represented in Figure 2.1, and also on the tire properties. The tire properties are related to the side slip angle, explained in more detail in Chapter 4, which is the angle between the rolling velocity of the wheel, in wheel plane, and its trajectory velocity.

There are two important scenarios to highlight related to the steering behaviour of the motorcycle: under-steering and over-steering. In under-steering, the side slip angle of the rear wheel is less than that of the front tire. In this scenario, the motorcycle describes a turn in a radius greater than the ideal one associated with the kinematic steering. If the under-steering becomes accentuated, it increases the risk of the front wheel losing the adherence. In over-steering, the side slip angle of the rear wheel is greater than the front tire. In this scenario, the motorcycle describes a turn in a radius smaller than the ideal one associated with the kinematic steering. If the over-steering becomes accentuated, the case now is different, there is a risk of the rear wheel losing the adherence.

It is interest to consider the case of a motorcycle entering in a curve, considering gyroscopic effects, which relates to the steering position of the motorcycle. Say that the motorcycle is to turn to a right curve. Contrary to the intuition, the handlebars are first turned to the left producing the effect of leaning the motorcycle to the right, due to the lateral force on the front wheel and gyroscopic moments. While entering the turn, the handlebars are slowly turned to the right to ensure the proper roll of the motorcycle in order to follow the required trajectory, i.e, to perform the right side curving.

Chapter 3

Multibody Dynamics Formulation

In this chapter, an overview of the multibody dynamics formulation is presented with the emphasis on the modelling and analysis of the motorcycle addressed in this work. Assuming that the flexibility of each one of the system components can be neglected, the analysis of a rigid body system allows calculating the forces acting on it. The procedure to identify the rigid bodies and to define the constraints between them is overviewed in order to describe the modeling facilities provided by the methodology used here. The forces applied on the motorcycle are also discussed, with particular interest on the contact forces of the tires.

3.1 Coordinates of the Multibody System

A rigid body uses six independent coordinates to represent its kinematics, being three for translation and three for rotation. Translation and rotation of a rigid body i, shown in Figure 3.1, is given by the position of its fixed frame (ξ, η, ζ) and the rotation of its axis relative to the global frame (X, Y, Z). Using Cartesian coordinates to define the position $\mathbf{r}_i = \begin{Bmatrix} x & y & z \end{Bmatrix}^T$ and Euler parameters to define the rotation $\mathbf{p}_i = \begin{Bmatrix} e_0 & e_1 & e_2 & e_3 \end{Bmatrix}^T$, in which one of the parameters is dependent [3]. The vector that defines the rigid body i position and orientation is $\mathbf{q}_i^* = \begin{Bmatrix} r_i^T & p_i^T \end{Bmatrix}^T$.

The position, in global coordinates, of a point P belonging to the rigid body i, is described by vector $\mathbf{r}_i$ written as:

$$\mathbf{r}_i^P = \mathbf{r}_i + \mathbf{s}_i^P = \mathbf{r}_i + \mathbf{A}_i \mathbf{s}_i'^P \tag{3.1}$$

where $\mathbf{A}_i$ is the transformation matrix from body i coordinates to the inertia frame coordinates,

$$\mathbf{A}_i = 2 \begin{bmatrix} e_0^2 + e_1^2 - \frac{1}{2} & e_1 e_2 - e_0 e_3 & e_1 e_3 + e_0 e_2 \\ e_1 e_2 + e_0 e_3 & e_0^2 + e_2^2 - \frac{1}{2} & e_2 e_3 - e_0 e_1 \\ e_1 e_3 - e_0 e_2 & e_2 e_3 + e_0 e_1 & e_0^2 + e_3^2 - \frac{1}{2} \end{bmatrix}_i \tag{3.2}$$

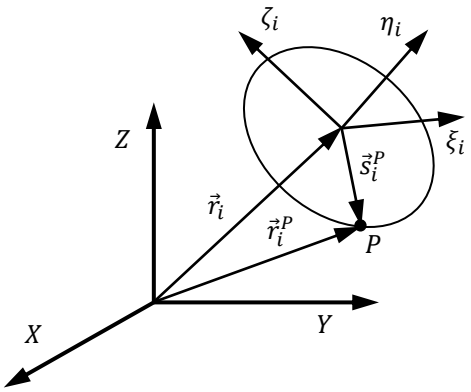

Figure 3.1: Position of a point P on a rigid body i.

The rigid body's local angular velocity is related to the time derivatives of Euler parameters $\dot{\mathbf{p}}_i$ by:

$$\dot{\mathbf{p}}_i = \frac{1}{2}\mathbf{L}_i\omega_i' \tag{3.3}$$

The transformation matrix $\mathbf{L}_i$, takes the form:

$$\mathbf{L}_i = \begin{bmatrix} -e_1 & e_0 & e_3 & -e_2 \\ -e_2 & -e_3 & e_0 & e_1 \\ -e_3 & e_2 & -e_1 & e_0 \end{bmatrix}_i \tag{3.4}$$

In order to keep track of the rigid bodies i kinematics, the position and orientation, velocity and acceleration of the rigid body is represented as:

$$\mathbf{q}_i^* = \begin{Bmatrix} \mathbf{r}_i^T & \mathbf{p}_i^T \end{Bmatrix}^T \quad \dot{\mathbf{q}}_i^* = \begin{Bmatrix} \dot{\mathbf{r}}_i^T & \omega_i'^T \end{Bmatrix}^T \quad \ddot{\mathbf{q}}_i^* = \begin{Bmatrix} \ddot{\mathbf{r}}_i^T & \dot{\omega}_i'^T \end{Bmatrix}^T \tag{3.5}$$

3.2 Kinematic Constraints

The kinematic constraints, representing the restrictions between the relative motion of the rigid bodies, are described by algebraic equations. These constraints are used to represent mechanical joints. By choosing the suitable kinematic joints, the behavior of a system of linked bodies can be modeled to satisfy the correct system mobility. In the case of application of this work, the motorcycle multibody model is described by two types of joints: revolute and translational joints.

3.2.1 Revolute Joint

Revolute joints, such as that in Figure 3.2 allow for a single rotation of two bodies around a common axis, thus preventing any other relative motion. This means that two parallel vectors on each body remain parallel after they move, always sharing a common point P.

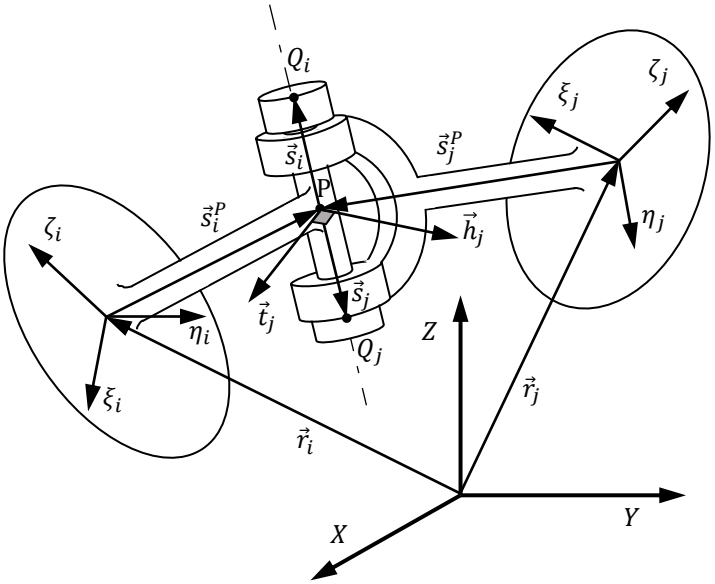

Figure 3.2: Revolute joint.

This joint has a single degree of freedom. Thus requiring five algebraic equations to represent the kinematic constraints. The relative translations are prevented by enforcing:

$$\mathbf{\Phi}^{(s,3)} \equiv \mathbf{r}_i + \mathbf{A}_i \mathbf{s}_i'^P - \mathbf{r}_j - \mathbf{A}_j \mathbf{s}_j'^P = 0 \tag{3.6}$$

The single rotation between the two bodies is allowed by constraining the two extra relative rotation. Let vectors $\mathbf{t}_j$ and $\mathbf{h}_j$ be perpendicular to $\mathbf{s}_j$ and between themselves, then the two extra constraints equations are set by:

$$\mathbf{\Phi}^{(p1,2)} \equiv \begin{Bmatrix} \mathbf{s}_j^T \mathbf{h}_j \\ \mathbf{s}_j^T \mathbf{t}_j \end{Bmatrix} = 0 \tag{3.7}$$

Note that another alternative formulation can be defined, but the one presented is used hereafter.

3.2.2 Translational Joint

Translational joints allow for the translation of two bodies through a common axis while preventing any relative rotation. The translational joint, represented in Figure 3.3, is defined by enforcing the orthogonality between different vectors.

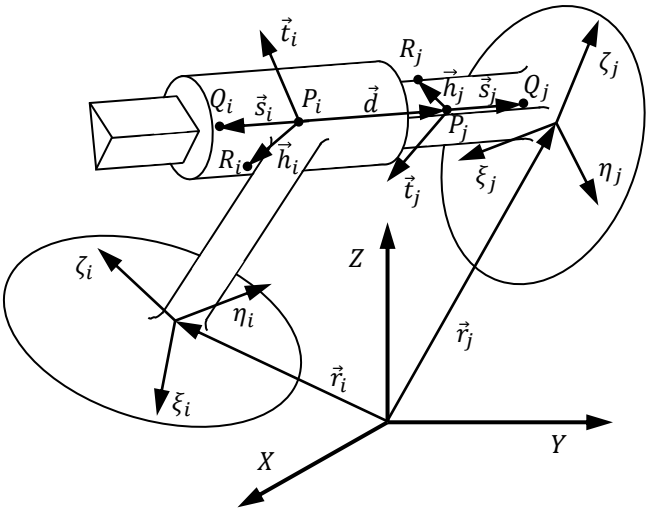

Figure 3.3: Translational joint.

This joint has also a single degree of freedom, being in this case a relative translation. Thus requiring five algebraic equations to represent the kinematic constraints. As similar as before, the two extra relative rotations are prevented by enforcing:

$$\mathbf{\Phi}^{(p1,2)} \equiv \begin{Bmatrix} \mathbf{t}_i^T \mathbf{s}_j \\ \mathbf{h}_i^T \mathbf{s}_j \end{Bmatrix} = 0 \tag{3.8}$$

To constraint the two others relative translations, vectors $\mathbf{t}_i$ and $\mathbf{h}_i$ are forced to be perpendicular to vector $\mathbf{d}$ defined by the points P_i and P_j. Then the two constraints are set by:

$$\mathbf{\Phi}^{(p2,2)} \equiv \begin{Bmatrix} \mathbf{t}_i^T \mathbf{d} \\ \mathbf{h}_i^T \mathbf{d} \end{Bmatrix} = 0 \tag{3.9}$$

To avoid the relative rotation of the two bodies, vectors $\mathbf{h}_i$ and $\mathbf{h}_j$ are also set as orthogonal, following the expression:

$$\mathbf{\Phi}^{(n1,1)} \equiv \mathbf{h}_i^T \mathbf{h}_j = 0 \tag{3.10}$$

3.2.3 Driver for Steering

For the purpose of motorcycle control, there is the need to define one more constraint. To control the steering with the handlebars, this constraint is defined as a driver constraint in a revolute joint.

Two vectors are given, $\mathbf{v}_i$ and $\mathbf{v}_j$, to regulate the angle δ between the two bodies in a revolute joint. The vector $\mathbf{v}_i$ is perpendicular to the vector $\mathbf{s}_i$, and $\mathbf{v}_j$ is perpendicular to $\mathbf{s}_j$. Vector $\mathbf{v}_j$ is also parallel to $\mathbf{v}_i$ when the two bodies are aligned, enforcing that the steering angle δ is null. To manage the angle δ, a cross product is used to define the constraint equation.

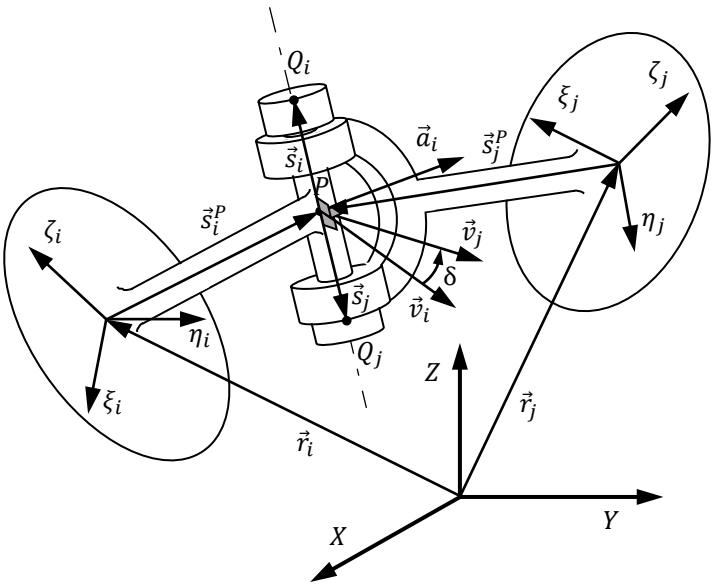

Figure 3.4: Driver for steering.

The driver is defined by a single algebraic constraint, which is the steering angle δ, related to the orientation of bodies i and j by:

$$\mathbf{\Phi}^{(sr,1)} \equiv \mathbf{a}_i^T \mathbf{v}_j - \sin(\delta) = 0 \tag{3.11}$$

In which the body fixed vector $\mathbf{a}_i$ is perpendicular to both $\mathbf{s}_i$ and $\mathbf{v}_i$. Note that the steering angle $\delta = \delta(t)$, being its time dependency given by the steering control strategy to be selected.

3.3 Equation of Motion

For any multi-body system, integrated with kinematic constraints and rigid bodies, the governing equilibrium equations are expressed as:

$$\begin{bmatrix} \mathbf{M} & \mathbf{\Phi}_q^T \\ \mathbf{\Phi}_q & 0 \end{bmatrix} \begin{Bmatrix} \ddot{\mathbf{q}} \\ \lambda \end{Bmatrix} = \begin{Bmatrix} \mathbf{g} \\ \boldsymbol{\gamma} - 2\alpha\dot{\mathbf{\Phi}} - \beta^2\mathbf{\Phi} \end{Bmatrix} \tag{3.12}$$

Here, $\mathbf{M}$ is the mass matrix, $\mathbf{\Phi}_q$ is the Jacobian matrix related to the kinematic constraints, $\ddot{\mathbf{q}}$ is the accelerations vector of the system, λ is the vector of Lagrange multipliers associated to the joints reaction forces, $\mathbf{g}$ is the force vector, $\boldsymbol{\gamma}$ is the right-hand side of the acceleration constraints equations, $\dot{\mathbf{\Phi}}$ is the first time derivative of the kinematic constraints $\mathbf{\Phi}$ and α and β are parameters associated with the Baumgarte Stabilization [10].

For a rigid body i, provided that the body fixed frame $(\xi, \eta, \zeta)_i$ is fixed to its center of mass and that the axis are coincident with its principal inertia axis, the matrix $\mathbf{M}_i$ is diagonal and filled with the mass and principal inertial moments of the body,

$$\mathbf{M}_i = \begin{bmatrix} m & & & & & \\ & m & & & & \\ & & m & & & \\ & & & I_{\xi\xi} & & \\ & & & & I_{\eta\eta} & \\ & & & & & I_{\zeta\zeta} \end{bmatrix}_i \tag{3.13}$$

The accelerations vector $\ddot{\mathbf{q}}_i$ of the rigid body i is composed by the translation accelerations $\ddot{x}$, $\ddot{y}$ and $\ddot{z}$, and angular accelerations expressed in the body fixed coordinates system $\dot{\omega}_\xi$, $\dot{\omega}_\eta$ and $\dot{\omega}_\zeta$.

$$\ddot{\mathbf{q}}_i = \begin{bmatrix} \ddot{x} & \ddot{y} & \ddot{z} & \dot{\omega}_\xi & \dot{\omega}_\eta & \dot{\omega}_\zeta \end{bmatrix}_i \tag{3.14}$$

To solve the system of equations in 3.12, it is necessary to set initial conditions. The parameter t_0 is the initial instant of time to start the simulation, $\mathbf{q}^*_{t_0} = \mathbf{q}^*_i$ the initial vector of position and orientation, and $\dot{\mathbf{q}}^*_{t_0} = \dot{\mathbf{q}}^*_i$ the initial velocity vector. The vectors $\mathbf{q}^*_i$ and $\dot{\mathbf{q}}^*_i$ are related via equation 3.5.

In order to understand and computationally implement the algorithm of the multibody equation of motion, a flowchart is shown in the Figure 3.5. The Baumgarte parameters are set to $\alpha = 5$ and $\beta = 5$, proving to be good values as suggested in [10].

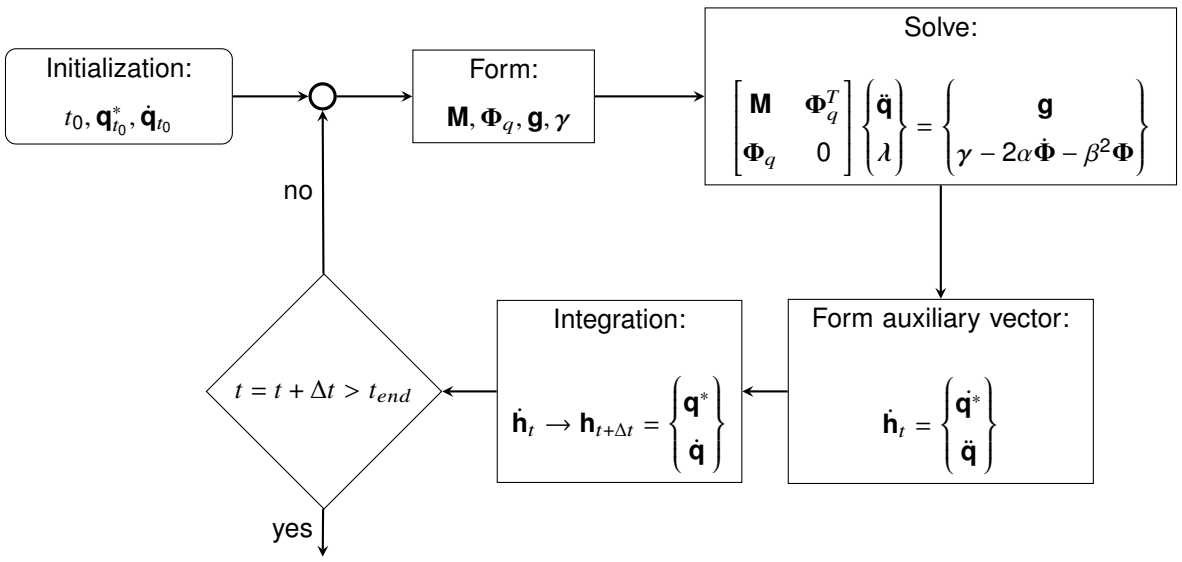

Figure 3.5: Flowchart of multibody dynamics program.

The forward dynamic analysis procedure proceeds by advancing the following steps:

Step 1: Set the initial conditions of the multibody model;

Step 2: Construct the matrices and vectors $\mathbf{M}$, $\mathbf{\Phi}_q$, $\boldsymbol{\gamma}$, $\mathbf{\Phi}$, $\dot{\mathbf{\Phi}}$ and $\mathbf{g}$;

Step 3: Solve the equations of motion to find $\ddot{q}$ and $\boldsymbol{\lambda}$;

Step 4: Determine the auxiliary vector $\dot{\mathbf{h}}_t = \begin{bmatrix} \dot{\mathbf{q}} & \ddot{\mathbf{q}} \end{bmatrix}^T$;

Step 5: Integrate vector $\dot{\mathbf{h}}_t$ to obtain $\mathbf{h}_{t+\Delta t}$;

Step 6: Update the time step $t = t + \Delta t$;

Step 7: Stop simulation if $t > t_{end}$, otherwise go to Step 2;

3.4 Applied Forces to the Multibody System

3.4.1 Suspension Systems Forces

The suspension has an important role in vehicle dynamics as the handling characteristics of the motorcycle strongly depend on them. The most important components of the suspension systems are translational spring-damper components such as that shown in Figure 3.6.

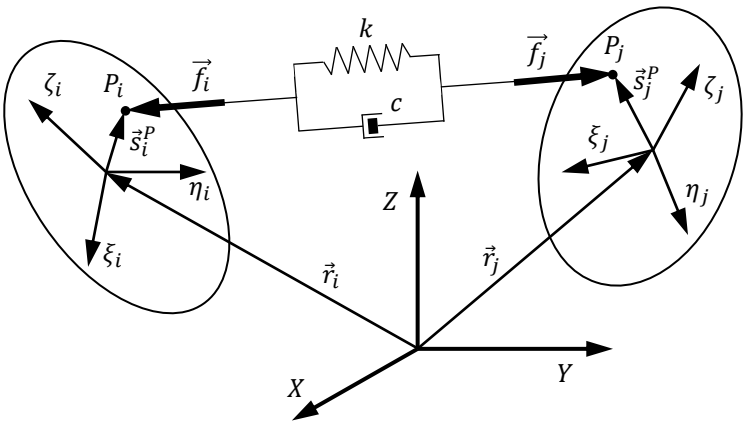

Figure 3.6: Spring-damper element between body i and j.

The force developed by the suspension element is computed through the sum of the spring and damper forces, f^k and f^c respectively. The force felt in body i is represented as:

$$\mathbf{f}_i^{kc} = \left(f_i^k + f_i^c \right) \mathbf{u} \tag{3.15}$$

while the force on body j is the opposite of that on the other body:

$$\mathbf{f}_j^{kc} = -\mathbf{f}_i^{kc} \tag{3.16}$$

Since body i and j are a reaction action pair, the forces felt in each body are equal in magnitude, but with different signal, as shown in the equation 3.16. The unit vector $\mathbf{u}$ is aligned with the points P of each body and is computed as $\mathbf{u} = \frac{\mathbf{d}}{\|\mathbf{d}\|}$, where $\mathbf{d}$ has the form of:

$$\mathbf{d} = \mathbf{r}_i + \mathbf{A}_i \mathbf{s}_i'^P - \mathbf{r}_j - \mathbf{A}_j \mathbf{s}_j'^P \tag{3.17}$$

The force computation of the spring in general, assuming this to be linear, is obtained by:

$$f^k = k\,(l_0 - l) \tag{3.18}$$

where k is the stiffness coefficient of the spring, l_0 is the undeformed length and l is given by $l = \sqrt{\mathbf{d}^T \mathbf{d}}$. To compute the force of the damper, its relation to the velocity in length is:

$$f^c = c\,\dot{l} \tag{3.19}$$

being c the damping coefficient and the vector $\dot{l}$ the rate of variation of the length between the P points. The vector is computed by $\dot{l} = \dot{d}^T u$, where $\dot{d}$, the velocity vector, takes the form of:

$$\dot{\mathbf{d}} = \dot{\mathbf{r}}_i + \mathbf{A}_i \tilde{\omega}_i' \mathbf{s}_i'^P - \dot{\mathbf{r}}_j - \mathbf{A}_j \tilde{\omega}_j' \mathbf{s}_j'^P \tag{3.20}$$

With all the quantities defined, the suspension force given by equation 3.15 is now formulated.

3.4.2 External Forces

Every type of systems are integrated on a medium, and the interaction between the system and the medium influences the system behaviour, beyond the internal forces developed inside the system. This interaction can be seen in a multibody system perspective, as external forces applied to it. For example, if the system is a ship, the environment is mostly composed of water, so the hydrodynamic forces are in great prominence. To model a ship, governing equations, such as the Navier-Stokes equation, are needed in order to describe the external forces applied.

For road vehicles, which are also affected by aerodynamic forces, the main interaction is usually with the road, that is relatively rigid. This interaction is commonly described by contact forces models [4, 5]. Contact between two bodies is often characterized by the normal and friction forces developed in each sliding body surface, and the stiffness and damping of the body that is treated as dissipative energy.

There are different contact force models to describe specific contact mechanism. The Kelvin-Voigt is a simple and discrete model for normal contact, while models based on Coulomb law are also frequently used to describe friction phenomenon [21]. When contact develops between rolling elements, deemed as rolling contact as described by Kalker [22], the constitutive equations of the contact mechanics are more intricate. Other sophisticated models were developed in description for the tire contact mechanism, as announced in [23].

In this work, the multibody system is a motorcycle and the contact is made between the road and the pneumatic tires, being the generic forces developed represented in Figure 3.7. Therefore, there is

the need to define a tire model to describe the rolling contact. Among the model options, two models are considered for the implementation: an analytical model developed by Gim and Nikravesh [6–8] and a semi-empirical one developed by Pacejka [9]. Among these, the Pacejka tire model is the mostly used by the industry and being its parameters available for the application foreseen here and, therefore, it is selected to be implemented in this work. Details about the model and its implementation are presented in Chapter 4.

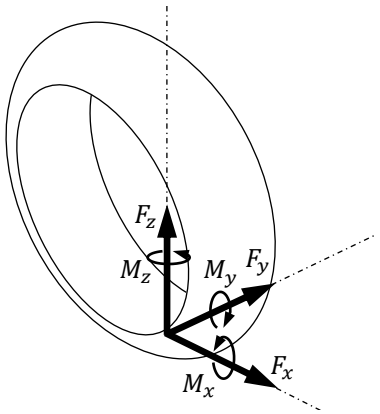

Figure 3.7: Forces and moments on pneumatic tire due to its interaction with the road.

Due to the rather complex details associated to the evaluation of the tire-road interaction forces, the complete evaluation methodology is presented in Chapter 4. The evaluation of the contact forces including the contact detection, tire forces evaluation and forces application are fully describe hereafter.

Chapter 4

Tire Forces Implementation

Tires have an important role on road vehicles, more specifically in their dynamics behaviour. They are the force elements that are in contact with the ground, where tire properties and geometry are of fundamental importance to evaluate moments of traction and braking. It is essential to use a model of the tire in the multibody model of the motorcycle to reflect a more realistic scenario on the application of forces and moments. The tire force evaluation requires that contact is first detected and, if it exists, that the proper kinematic quantities of the wheel and road are defined. Afterwards, the tire force model is used to evaluate the tire forces and moments.

In this chapter, the tire model known as *Pacejka Magic Formula* developed in [9] is presented with the assumptions purposed by Sharp [11]. The implementation of the *Pacejka Magic Formula* tire model is presented and the demonstration of its performance compared with of the [11]. Finally, the tire contact forces are applied to the wheel body in which the tire is mounted.

4.1 Contact Detection

The contact detection is the first step on tire forces calculation. Since the simulation is done in a selected track, the track construction is assumed to be done by triangular patches. The contact search consists in identifying the contact patch and evaluating an indentation between the tire geometry and road. The unevenness of the ground is well described by a triangular mesh. Each triangle is represented by three nodes numbered counterclockwise with respect to the normal of the triangle surface $\mathbf{u}_n$, as shown in Figure 4.1.

For every time step in contact detection algorithm, two main parts are identified. First it is assumed a flat horizontal road, and after the search for a triangular contact patch, all the quantities needed for the tire model are computed if there is penetration of the tire with the road. Second, if the triangular contact patch found is not horizontal, the quantities are computed again for the new triangular contact path. For future explanations of these main parts, Figure 4.2 reveals all the points, referential systems and quantities needed for better understanding.

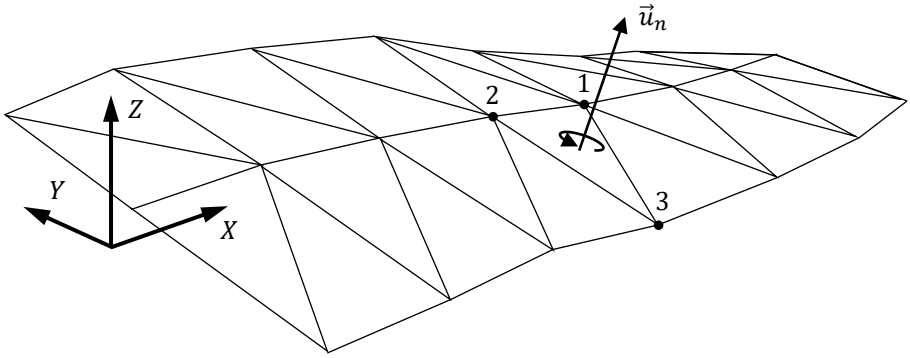

Figure 4.1: Representation of the road by a triangular mesh.

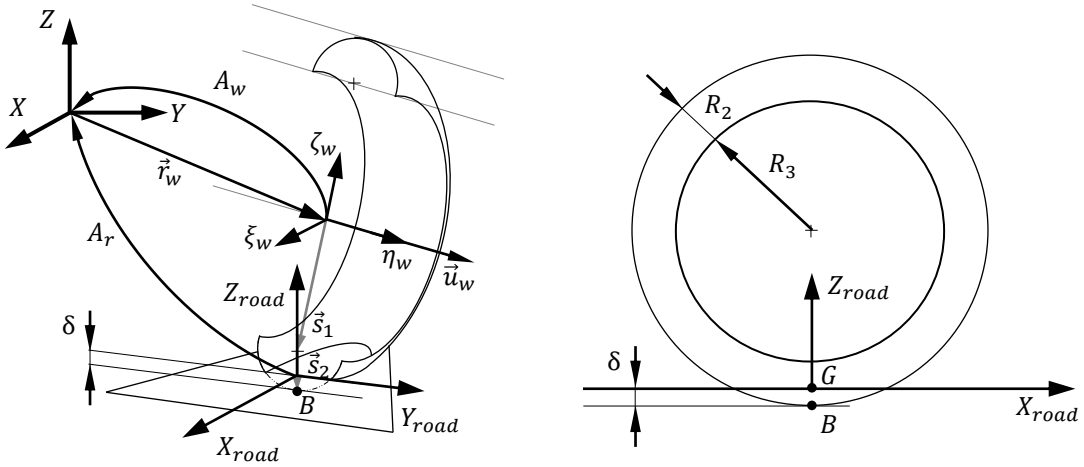

Figure 4.2: Axis system necessary and important points in contact search.

It is relevant how tire geometry is defined. Figure 4.2 shows that the tire can be approximated to a toroidal body, with a revolution R_3, of a crown with radius R_2. Point G is the contact point with the road, not the one used later for the tire model, and B the point below, belonging to the crown surface. On the limit of the contact, B and G are the same.

In order to search for a triangular contact patch, the position of point B is firstly defined by equation 4.1, assuming a flat road. The matrix $\mathbf{A}_r = \begin{bmatrix} \mathbf{u}_{xr} & \mathbf{u}_{yr} & \mathbf{u}_{zr} \end{bmatrix}$, represents the transformation matrix of the road coordinate system $(XYZ)_{road}$ to the global coordinate system (XYZ). Assuming for instance an horizontal road, the matrix $\mathbf{A}_r$ in this case is defined in way that vector $\mathbf{u}_{xr}$ is parallel and orientated to the axis ξ_w of the fixed frame body wheel, and $\mathbf{u}_{zr}$ has the same direction and orientation of global axis Z:

$$\begin{aligned} \mathbf{r}^B &= \mathbf{r}_w + \mathbf{s}_1 + \mathbf{s}_1 \\ \mathbf{s}_1 &= R_3 \tilde{\mathbf{u}}_w \mathbf{u}_{xr} \\ \mathbf{s}_2 &= -R_2 \begin{Bmatrix} 0 \\ 0 \\ 1 \end{Bmatrix} \end{aligned} \tag{4.1}$$

where the unit vector $\mathbf{u}_w$, perpendicular to the tire plane, is defined as $\mathbf{u}_w = \mathbf{A}_w \begin{Bmatrix} 0 & 1 & 0 \end{Bmatrix}^T$ and $\mathbf{A}_w$ is the transformation matrix from the wheel body to the global coordinate system. The unit vector $\mathbf{u}_{xr}$ is expressed as:

$$\begin{aligned} \mathbf{u}_{xr} &= \frac{\tilde{\mathbf{u}}_w \mathbf{u}_{zr}}{\|\tilde{\mathbf{u}}_w \mathbf{u}_{zr}\|} \\ \mathbf{u}_{zr} &= \begin{Bmatrix} 0 \\ 0 \\ 1 \end{Bmatrix} \end{aligned} \tag{4.2}$$

Having the first approximation of point B coordinates, the searching for the a triangular contact patch can now proceed. Since every triangular patch has its nodes coordinates information and the respective normal to the surface, coordinates of point B are compared with all the contact patches just in the first time step. The equations 4.3 and 4.4 shows how the searching proceeds, where first is delimited a searching square and then looking for the triangular contact patches inside of this square.

$$\begin{aligned} X_{min} \leq x_B \leq X_{max} \\ Y_{min} \leq y_B \leq Y_{max} \end{aligned} \tag{4.3}$$

$$\begin{aligned} \sin(\alpha_1) &= s_{1B(y)} s_{12(x)} - s_{1B(x)} s_{12(y)} \geq 0 \\ \sin(\alpha_2) &= s_{2B(y)} s_{23(x)} - s_{2B(x)} s_{23(y)} \geq 0 \\ \sin(\alpha_3) &= s_{3B(y)} s_{31(x)} - s_{3B(x)} s_{31(y)} \geq 0 \end{aligned} \tag{4.4}$$

Being the coordinates of the nodes represented by (X, Y), the conditions of equation 4.4 are only verified if equation 4.3 is confirmed. For the next time steps the search is not done on all the triangular contact patches. First, it is checked if the triangular contact patch of the previous time step is still the same, if not, the search is made in a first proximity ring of the previous triangle. If it is not found in this first proximity ring, the search moves to a second proximity ring, as shown in the Figure 4.4. The searching is also done by the computation of equations 4.3 and 4.4. The time step used for the search can be adjusted to ensure that the tire does not pass the search zone. Note that each triangle has the information of proximity rings stored.

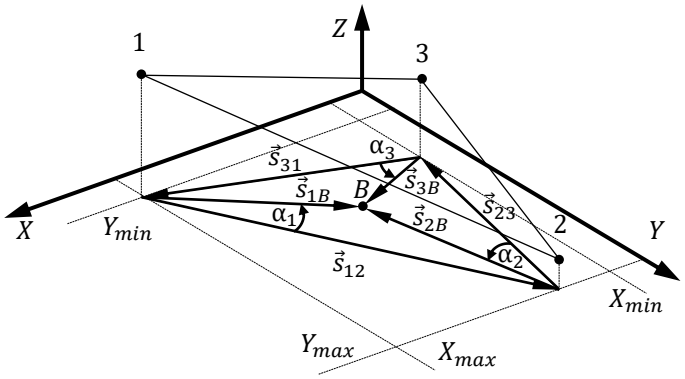

Figure 4.3: Determination of triangular contact patch.

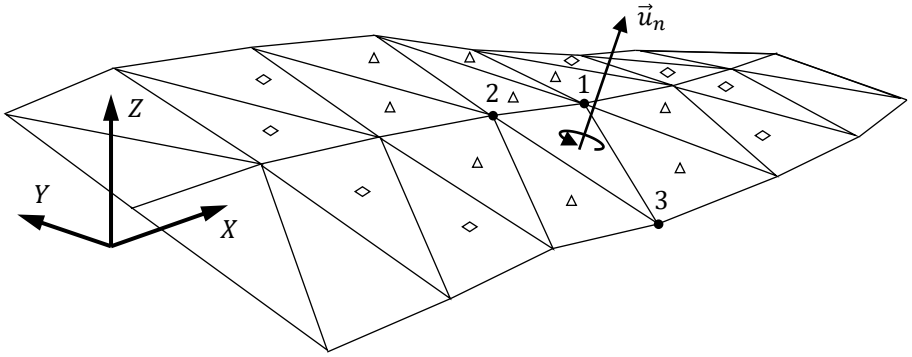

Figure 4.4: Rings of proximity for contact verification. First ring identified by △ and second by □.

For a Flat Horizontal Road

If the possible triangular contact path found is horizontal, $\mathbf{u}_n = \begin{Bmatrix} 0 & 0 & 1 \end{Bmatrix}^T$, the penetration δ between the tire and the contact patch is evaluated by performing:

$$\delta = z^G - z^B \tag{4.5}$$

The quantities z^G and z^B are the z coordinates of point G and B, respectively. The quantity z^B is known from equation 4.1 while the quantity z^G is obtained from the expression which defines a plan as:

$$z^G = a + bx^B + cy^B \tag{4.6}$$

where a, b and c are the plan coefficients. Note that $x^G = x^B$ and $y^G = y^B$, since the triangular contact path found is horizontal. There is penetration between the tire and the road if $\delta > 0$, otherwise the search is initiated for the other tire and then advance for the next time step. The penetration δ, the position of the contact point $\mathbf{r}^G = \begin{Bmatrix} x^G & y^G & z^G \end{Bmatrix}^T$ and the transformation matrix $\mathbf{A}_r$ are now defined for the case of having a horizontal contact patch.

For a Non-Horizontal Road

If the contact patch found is not horizontal, $\mathbf{u}_n \neq \begin{Bmatrix} 0 & 0 & 1 \end{Bmatrix}^T$, the coordinates of point B need to be recalculated. The transformation matrix $\mathbf{A}_r = \begin{bmatrix} \mathbf{u}_{xr} & \mathbf{u}_{yr} & \mathbf{u}_{zr} \end{bmatrix}$ is redefined by equation 4.7, knowing the normal vector $\mathbf{u}_n$ of the triangular contact patch found.

$$\begin{aligned} \mathbf{u}_{zr} &= \mathbf{u}_n \\ \mathbf{u}_{xr} &= \frac{\tilde{\mathbf{u}}_w \mathbf{u}_{zr}}{\|\tilde{\mathbf{u}}_w \mathbf{u}_{zr}\|} \\ \mathbf{u}_{yr} &= \tilde{\mathbf{u}}_{zr} \mathbf{u}_{xr} \end{aligned} \tag{4.7}$$

In equation 4.8, the symbol ´ refers to coordinates that are taken from local road axis. With the transformation matrix $\mathbf{A}_r$ redefined, the point B is recalculated for the non-horizontal triangular contact patch by performing:

$$
\begin{aligned}
\mathbf{r}^B = \mathbf{A}_r \mathbf{r}'^B &= \mathbf{A}_r (\mathbf{A}_r^T \mathbf{r}_w + \mathbf{s}'_1 + \mathbf{s}'_2) \\
\mathbf{s}'_1 &= R_3 \begin{Bmatrix} 0 \\ \mathbf{u}'_{w(z)} \\ -\mathbf{u}'_{w(y)} \end{Bmatrix} \\
\mathbf{s}'_2 &= -R_2 \begin{Bmatrix} 0 \\ 0 \\ 1 \end{Bmatrix}
\end{aligned}
\tag{4.8}
$$

To evaluate the penetration δ for the case of a non-horizontal contact patch, the equation 4.9 is used, where the coordinate z of the normal vector $\mathbf{u}_n$ of the contact patch is multiplied by the equation 4.5, following the expression:

$$
\delta = \mathbf{u}_{n(z)} (z^G - z^B) \tag{4.9}
$$

The contact is again verified if the rigid body wheel penetrates the road with $\delta > 0$, as illustrated in Figure 4.2. In order to compute the position of the contact point $\mathbf{r}^G$, equation 4.10 is given as:

$$
\mathbf{r}^G = \mathbf{r}^B + \delta \mathbf{u}_n \tag{4.10}
$$

For the case of the non-horizontal triangular contact patch, are defined the value of the penetration δ, the position of the contact point $\mathbf{r}^G$ and the transformation matrix $\mathbf{A}_r$. Described the contact detection of the tire with the road, the kinematic quantities used for the tire model can be computed.

Underlining a unique situation, the new computation of the point B coordinates could reveal that the point B is in fact in other contact patch. This may occur if the contact exists close to the border of a triangular patch. Therefore, the searching procedure for a new contact patch could be repeated again to ensure that the contact is made with the correct contact patch.

4.2 Kinematic Quantities for Pacejka Magic Formula

The computation of the kinematic quantities to evaluate the forces acted on the tire, are common to some model, as [6–8] and [9]. Therefore, Figure 4.5 shows the important angles on tire dynamics used to compute the necessary kinematic quantities.

In order to calculate the slip quantities, it is important to understand how Pacejka defines the tire. The tire is seen as a thin disc, where the point C, shown in Figure 4.6, is the contact center point intersected by the disc and road. Point S, shown in Figure 4.6, is located at a distance from the wheel center equal to the effective radius r_e, function of intrinsic parameters to each tire.

$$
r_e = r_0 - \frac{F_{z0}}{C_z} \left\{ D_{reff} \arctan\left(B_{reff} \frac{C_z}{F_{z0}} \delta \right) + F_{reff} \frac{C_z}{F_{z0}} \delta \right\} \tag{4.11}
$$

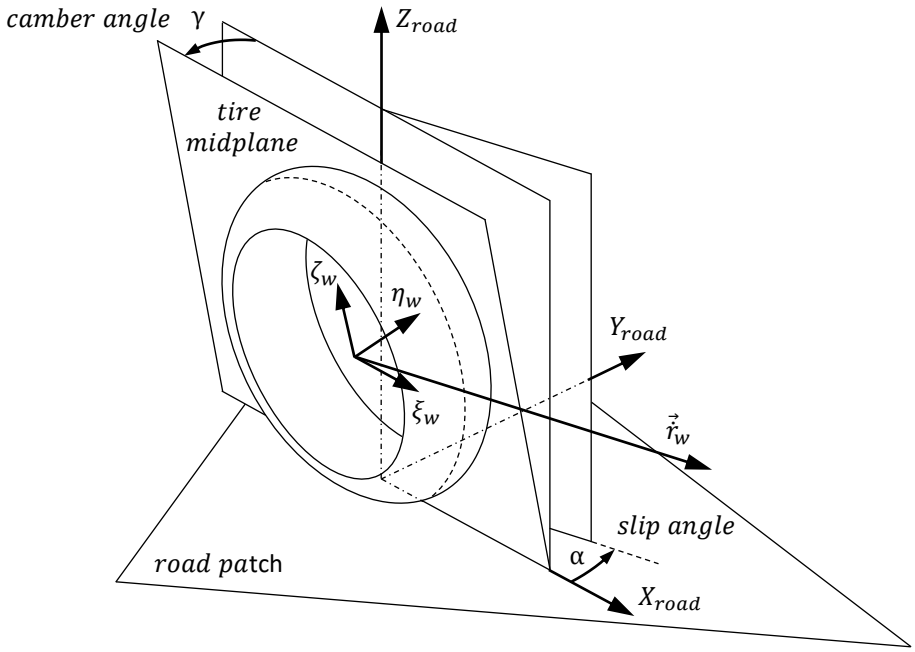

Figure 4.5: Important angles in tire dynamics.

In the expression 4.11, the centrifugal growth of the tire is not taking into account. F_{z0} is the nominal force considered, C_z the radial stiffness coefficient, $r_0 = R_2$+R_3 the unloaded radius and δ the penetration value. The other tire parameters D_{reff}, B_{reff} and F_{reff} are taken from the tire data presented in appendix B.

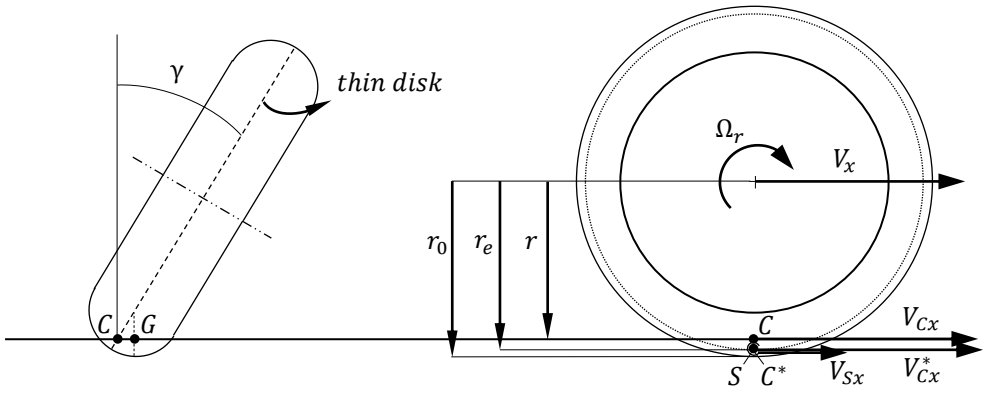

Figure 4.6: Location of point C, its velocity and slip velocity on point S (adapted from [9]).

For Pacejka, the slip quantities are evaluated around point C. To compute the position of point $\mathbf{s}_w^C$ with respect to the wheel center of mass, given by equation 4.12, is considered the position of the contact point G computed before.

$$\mathbf{s}_w^C = \mathbf{s}_w^G + \mathbf{A}_r \left\{ (R_2 - \delta) \tan(\gamma) \right\} \mathbf{u}_y \tag{4.12}$$

where $\mathbf{u}_y = \begin{Bmatrix} 0 & 1 & 0 \end{Bmatrix}^T$.

The position of the contact point $\mathbf{s}_w^G$ with respect to the wheel center of mass is given by $\mathbf{s}_w^G = \mathbf{r}^G - \mathbf{r}_w$ and γ is in fact the camber angle value expressed by equation 4.17. Having established the necessary

points, slip quantities are ready to be computed. Longitudinal slip κ is given as the quotient between the longitudinal slip velocity V_{Sx} and longitudinal velocity V_{Cx}:

$$\kappa = -\frac{V_{Sx}}{max[|V_{Cx}|, \varepsilon_{Vx}]} \tag{4.13}$$

Cases where the velocity V_{cx} becomes null, it is replaced for a small quantity $\varepsilon_{Vx} = 10^{-3}$, also to calculate lateral slip ratio. The longitudinal slip velocity, i.e., longitudinal velocity of point S, is given as $V_{Sx} = V_{Cx} - V_r$, where V_{Cx} is the longitudinal running velocity in point C and $V_r = \Omega_r r_e$ the rolling velocity, where Ω_r, seen in Figure 4.6, is the angular rolling velocity of the wheel. When $\gamma\dot{\psi} = 0$, meaning no yaw rate or camber angle, the velocity V_{cx} is equal to the longitudinal velocity of the wheel center V_x. Covering all cases, V_{Cx} can be computed as follow, where ω_w is the angular velocity of the wheel.

$$V_{Cx} = (\mathbf{A}_r^T \dot{\mathbf{r}}_w)^T \mathbf{u}_x - (\mathbf{A}_r^T \boldsymbol{\omega}_w)^T \mathbf{u}_z \left\|\mathbf{s}_w^C\right\| \sin(\gamma) \tag{4.14}$$

where $\mathbf{u}_x = \begin{Bmatrix} 1 & 0 & 0 \end{Bmatrix}^T$ and $\mathbf{u}_z = \begin{Bmatrix} 0 & 0 & 1 \end{Bmatrix}^T$.

For a flat (or approximately flat) road, there is no angular variation between point S and wheel center. Lateral slip ratio α^* is defined as the tangent of the slip angle, computed as the quotient between lateral slip velocity V_{sy} and longitudinal velocity of point C. Using the modulus for V_{Cx}, backwards running is covered.

$$\alpha^* = \tan\alpha \cdot sgn(V_{Cx}) = \frac{V_{Sy}}{max[|V_{Cx}|, \varepsilon_{Vx}]} \tag{4.15}$$

V_{Sy} can be obtained as follows:

$$V_{Sy} = (\mathbf{A}_r^T \dot{\mathbf{r}}_w)^T \mathbf{u}_y + \left(\mathbf{A}_r^T r_e \tilde{\mathbf{u}}_z \omega_w\right)^T \mathbf{u}_y \tag{4.16}$$

The value of camber angle, the resulting angle between the normal of the road and the thin disc, can be computed as:

$$\gamma = \frac{\pi}{2} - \arccos(\mathbf{u}_w^T \mathbf{A}_r \mathbf{u}_z) \tag{4.17}$$

Performed the computation of slip quantities - longitudinal slip κ, lateral slip α^* and the camber angle γ - the *Pacejka Magic Formula* will be used to ensure the forces developed on the tire.

4.3 Pacejka Magic Formula

If there is contact between tire and road, the tire model chosen can now be applied. Pacejka tire model, described in [9], is a ”semi-empirical” approach due to its duality of using experimentally measured data and having, at the same time, a structure often found in physical models. Pacejka tire model, also called *Magic Formula*, was initially developed for cars or other similar vehicles, not taking into account large roll angles. In order to model motorcycles, Pacejka developed an adaptation of the original formula. Sharp [11] presents an excellent explanation on tire parameterization, as well as simplification of expressions

of the model. It also presents some helpful examples for setting values for tire parameter to achieve, for instance, symmetric tire.

The model used in this chapter is restricted for steady-state situation. The inputs necessary for the model are presented in the Table 4.1, as well as their outputs.

Table 4.1: Input variables necessary for the model and the outputs given.

Input	Output
longitudinal slip ratio, κ	F_x
lateral slip ratio, α^*	F_y
camber angle, γ	M_x
F_z	M_y
	M_z

The model is known by *Magic Formula*, because it is the used a single standard formula to compute different output values. Besides the input described in the table, the formula also needs non-dimensional parameters p, q, r and s, related to the tire used and some operation condition, and a set of scaling factors λ. The default values of λ presented in Pacejka [9] will be considered. Herewith, high friction surface is considered since the parameters $\lambda_{\mu x}$ and $\lambda_{\mu y}$ responsible for the coefficient friction on x and y direction, respectively, are equal to 1.

The equations used to compute the output values for this work are given in appendix A. It is important to refer that the equations refer to the *Magic Formula* for motorcycle. Next equations show the general formula developed in [9].

$$y = D \sin\left[C \arctan\left\{Bx - E\left(Bx - \arctan Bx\right)\right\}\right] \tag{4.18}$$

$$Y(X) = y(x) + S_V \tag{4.19}$$

$$x = X + S_H \tag{4.20}$$

where

- Y output variables F_x, F_y or M_z
- X input variables $\tan(\alpha)$ or κ

and

- B stiffness factor
- C shape factor
- D peak value

- E curvature factor
- S_H horizontal shift
- S_V vertical shift

Together with the kinematic quantities calculated in the previous section, the tire model also needs the vertical force F_z imposed on the tire as input. The vertical force F_z, needed to compute the remaining forces and moments, can be expressed by the distance and velocity penetration, δ and $\dot{\delta}$ respectively. C_z is the radial stiffness coefficient of the tire and D_z its radial damping coefficient. The expression of the vertical force is presented as follows, with a different form from the one used in [9].

$$F_z = C_z\delta - D_z\dot{\delta} \tag{4.21}$$

Proceeding to the computation of the forces vector $\mathbf{f} = \begin{Bmatrix} F_x & F_y & F_z \end{Bmatrix}^T$ as well as the moments vector $\mathbf{m} = \begin{Bmatrix} M_x & M_y & M_z \end{Bmatrix}^T$, with the use of the expressions contained in Appendix A, the outputs of the tire model are all defined. To ensure that the computed forces and moments are correct, graphs were made using the tire proprieties of 180/55 taken from *Adams* software. The shape of the graphs are compared with [11], keeping in mind that ISO norm is used in this work. To work with a symmetric tire model, the following coefficients were set to zero [11], modifying some of the original tire parameters presented in Appendix B.

$$S_{Hx\alpha} = S_{Hy\kappa} = S_{Vy\kappa} = 0 \tag{4.22}$$

The nominal force $F_{z0} = 1200N$ is the value used based on the typical value of the tire, considering the mass of the motorcycle model. The values of the forward velocity $V_x = 20m/s$ and the tire unloaded radius $r_0 = 0.3m$ are also chosen. Next graphs show the forces and moments in function of input parameters for a given tire properties.

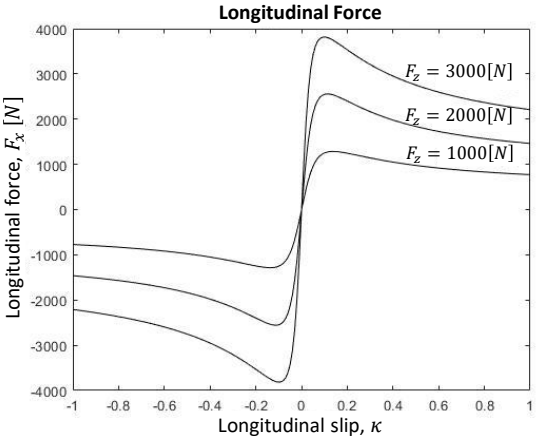

Figure 4.7: Tire longitudinal force in pure slip ($\alpha = \gamma = 0$), F_{x0}.

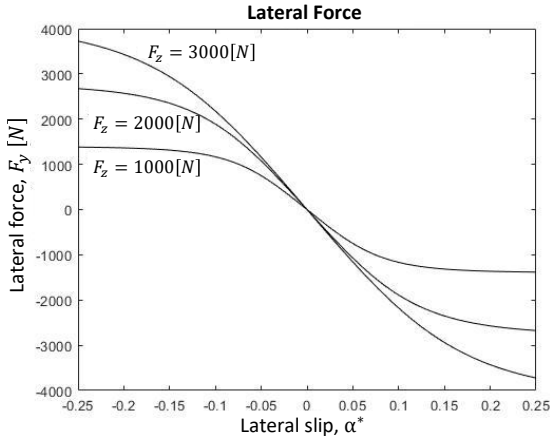

Figure 4.8: Tire lateral force in pure slip ($\kappa = \gamma = 0$), F_{y0}.

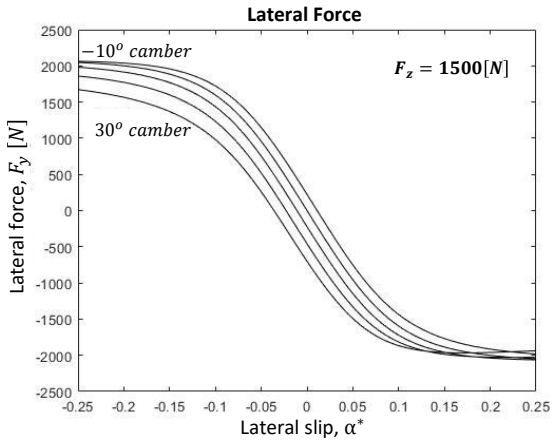

Figure 4.9: Tire lateral force in pure slip ($\kappa = 0$), F_{y0}. Camber angle values $-10°, 0°, 10°, 20°, 30°$.

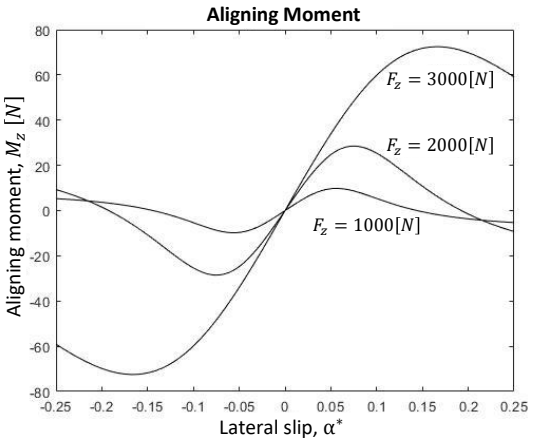

Figure 4.10: Tire aligning moment in pure slip ($\kappa = \gamma = 0$), M_{z0}.

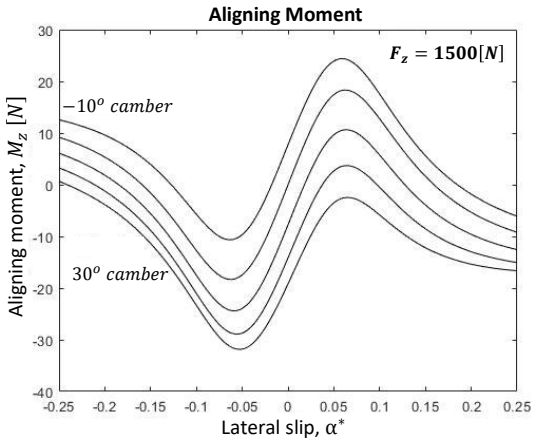

Figure 4.11: Tire aligning moment in pure slip ($\kappa = 0$), M_{z0}. Camber angle values, $-10°$, $0°$, $10°$, $20°$, $30°$.

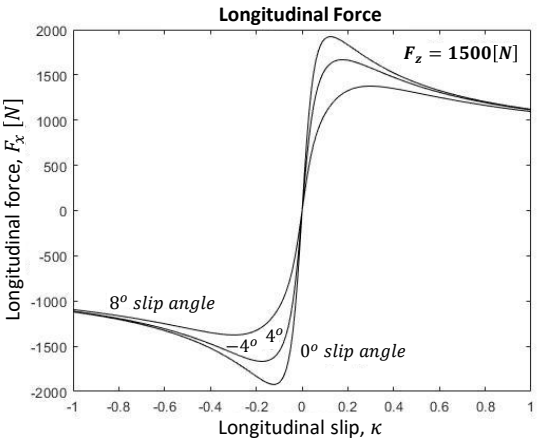

Figure 4.12: Tire longitudinal force in combined slip ($\gamma = 0$), F_x. Slip angle values,$-4°$, $0°$, $4°$, $8°$. The lines for $-4°$ and $4°$ are the same.

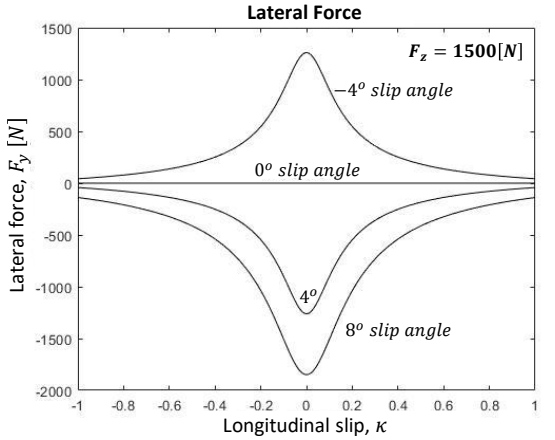

Figure 4.13: Tire lateral force in combined slip ($\gamma = 0$), F_y. Slip angle values, $-4°, 0°, 4°, 8°$.

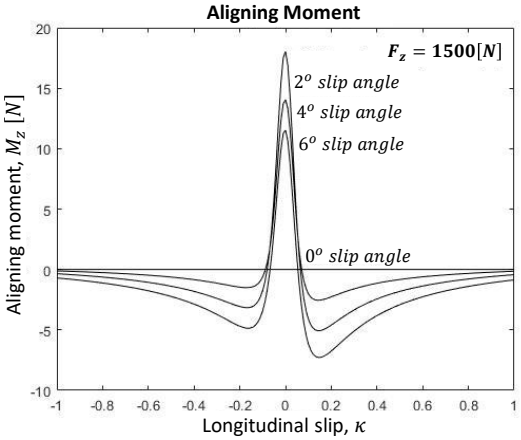

Figure 4.14: Tire aligning moment in combined slip ($\gamma = 0$), M_z. Slip angle values, $0°, 2°, 4°, 6°$.

All the graphs have a similar shape to the graphs presented in [11]. The values of the peaks in Figure 4.10 are slightly higher, compared with [11], because of the vertical nominal force F_{z0} chosen. In the case of Figure 4.14, the aligning moment is not symmetric on a line for a longitudinal slip value of $\kappa = 0$, because the moment is taken from point C and not from point G. This difference is observed due to the term $s \cdot F_x$, in the expression of M_z, defined in the section Appendix A.2.5.

4.4 Transfer Forces to the Body Wheel

With all the outputs expressed, the vector of forces $\mathbf{f} = \begin{Bmatrix} F_x & F_y & F_z \end{Bmatrix}^T$ and moments $\mathbf{m} = \begin{Bmatrix} M_x & M_y & M_z \end{Bmatrix}^T$ resultant on point C are transferred for the wheel body center of mass, in order to incorporate the **g** forces vector of the multibody system dynamics, as seen in Figure 3.5. Performing the following equation, the force vector **f** is transported to the wheel center of mass with the respective moments associated.

$$\begin{aligned} \mathbf{g} &= \mathbf{g} + \begin{Bmatrix} \mathbf{g}_f^T & \mathbf{g}_m^T \end{Bmatrix}^T \\ \mathbf{g}_f &= \mathbf{A}_r \mathbf{f} \\ \mathbf{g}_m &= \mathbf{A}_w^T \tilde{\mathbf{s}}_w^C \left(\mathbf{A}_w^T \mathbf{A}_r \mathbf{f} \right) \end{aligned} \tag{4.23}$$

Finally, the vector **g** associated to the tire model is completely define by adding the vector of moments **m** through the expression:

$$\begin{aligned} \mathbf{g} &= \mathbf{g} + \begin{Bmatrix} \mathbf{0}^T & \mathbf{g}_M^T \end{Bmatrix}^T \\ \mathbf{g}_M &= \mathbf{A}_w^T \mathbf{A}_r \mathbf{m} \end{aligned} \tag{4.24}$$

where $\mathbf{0}^T = \begin{Bmatrix} 0 & 0 & 0 \end{Bmatrix}^T$.

Following the entire procedure described in the present Chapter, the contact forces developed on each tire, which is mounted on the wheel body, can now be applied to the entire motorcycle model with the perspective of applying external forces to the dynamic system.

Chapter 5

Multibody Model for the Motorcycle

In this chapter it will be presented the multibody model constructed for the motorcycle TLM03e. All the multibody formulation made in Chapter 3 will be used to present the values needed in order to characterize the rigid bodies, kinematic joints, suspension elements and tires. Finally, a simple scenario with the motorcycle model is presented.

5.1 Description of TLM03e

TLM03e is a racing track motorcycle developed by TLMoto team, a group of enthusiastic students for motorcycle engineering from Instituto Superior Técnico. The TLM03e is an electric motorcycle, developed with the aim of participating in an international competition called Motostudent. In order to be prepared for all the competition challenges, TLM03e has the ability to be adjusted to improve its performance.

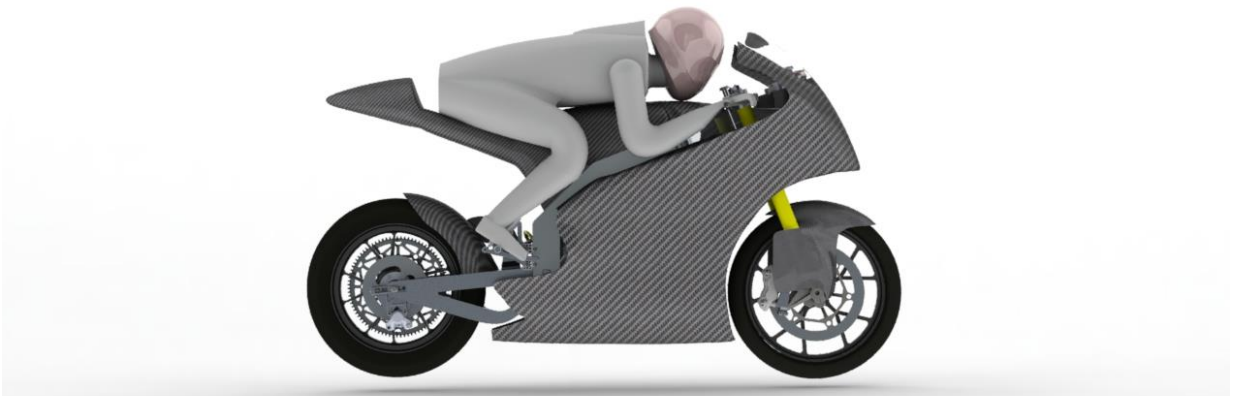

Figure 5.1: TLM03e CAD.

TLM03e has an aluminum twin-spar frame and an aluminum swingarm. All the fairings and the seat are made with carbon fiber composite. Since TLM03e is a racing track motorcycle, mirrors and lights are not included.

Table 5.1: General specifications of TLM03e.

General specifications	
Max. Power	42 $[kw]$
Top speed (default)	180 $[km/h]$
Mass	150 $[kg]$

5.2 Multibody Model

To obtain the necessary values for the multibody model, a CAD software with the entire motorcycle is used to have a more accurate and faster acquisition of data. The data is taken considering the motorcycle hanging, in other words, no force applied by the suspension elements, and with the default mechanical setup.

5.2.1 Rigid Bodies

The motorcycle multibody model is composed of 6 rigid bodies where the rear suspension is not taking into account, since it has a very low weight. For dynamics purposes, body 3 is composed for the pilot, in a static position, and frame. It is assumed $80kg$ for the pilot's weight. According to the general geometric parameters commonly used to describe a motorcycle, Table 5.2 presents the default values of TLM03e. Table 5.3 shows the mass properties and the principal moments of inertia of each rigid body.

Table 5.2: Geometric parameters of TLM03e.

Geometric parameters	
wheelbase, p	1.407 $[m]$
rake angle, τ	22.9 [deg]
trail, a	0.094 $[m]$
forward offset, d	0.026 $[m]$

Table 5.3: Body mass and moments of inertia.

Body	Mass $[kg]$	$I_{\xi\xi}$ $[kg.m^2]$	$I_{\eta\eta}$ $[kg.m^2]$	$I_{\zeta\zeta}$ $[kg.m^2]$
1. Rear Wheel	9.11	0.19	0.35	0.19
2. Swingarm	5.67	0.08	0.19	0.24
3. Frame + Pilot	185.06	17.47	22.58	9.99
4. Front Sprung	9.88	0.37	0.26	0.11
5. Front Unsprung	5.29	0.08	0.04	0.06
6. Front Wheel	6.88	0.10	0.19	0.10
7. Ground	-	-	-	-

To get the coordinates of position and orientation of each rigid body, it is assumed that the centers of mass of each body are in the motorcycle midplane, coincident with the XZ global plane. The position of the motorcycle relative to the global coordinates system can be seen in Figure 5.2, where the Z axis is coincident with the rear tire and the X axis is coincident with both tires.

For each rigid body, the local coordinates system is positioned in its center of mass and aligned with the principal axis of inertia. Table 5.4 presents the coordinates of position and orientation of each rigid body.

Table 5.4: Centers of mass position (global coordinates) and orientations (Euler parameters).

Body	X $[m]$	Y $[m]$	Z $[m]$	e_1	e_2	e_3
1. Rear Wheel	0.300	0.000	0.300	0.000	0.000	0.000
2. Swingarm	0.544	0.000	0.304	0.000	-0.063	0.000
3. Frame + Pilot	0.987	0.000	0.741	0.000	-0.368	0.000
4. Front Sprung	1.489	0.000	0.801	0.000	-0.199	0.000
5. Front Unsprung	1.662	0.000	0.327	0.000	-0.199	0.000
6. Front Wheel	1.707	0.000	0.290	0.000	0.000	0.000
7. Ground	0.000	0.000	0.000	0.000	0.000	0.000

In order to simplify, it is also assumed that the η principal axis of inertia of each rigid body is normal to the XZ plane. Compared with the real principal axis of inertia, this assumption in its orientation is almost imperceptible.

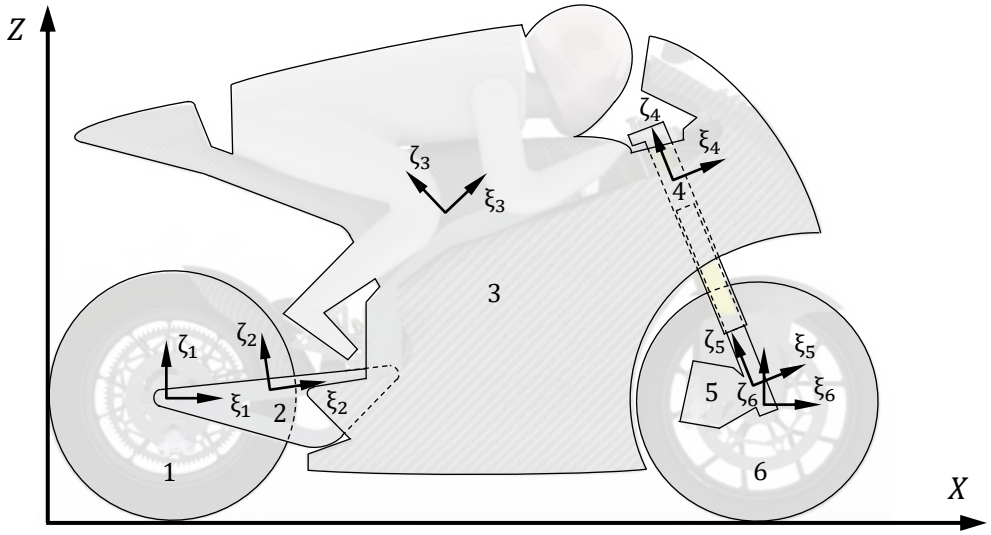

Figure 5.2: Bodies position and its local coordinates system.

5.2.2 Kinematic Joints

The kinematic joints are responsible for giving the bodies the desired motion between them. With all the bodies defined in Section 5.2.1, kinematic constraints can now be formulated in order to link the rigid bodies, as shown in Table 5.5.

Table 5.5: Formulation of Kinematic Joints.

Joint	Body i	Body j	$(\xi/\eta/\zeta)_i^P$ $(\xi/\eta/\zeta)_i^Q$ $[m]$	$(\xi/\eta/\zeta)_j^P$ $(\xi/\eta/\zeta)_j^Q$ $[m]$
R1. Rear Wheel/Swingarm	1	2	0/0/0 0/1/0	-0.242/0/0.027 -0.242/1/0.027
R2. Swingarm/Frame + Pilot	2	3	0.264/0/0.027 0.264/1/0.027	-0.394/0/-0.148 -0.394/1/-0.148
R3. Frame + Pilot/Front Sprung	3	4	0.435/0/-0.1485 0.390/0/-0.2685	-0.026/0/0 -0.026/0/-1
R4. Front Unsprung/Front Wheel	5	6	0.028/0/-0.051 0.028/1/-0.051	0/0/0 0/1/0
T1. Front Sprung/Front Unsprung	4	5	0.0015/0/0 0.0015/0/-1	0.028/0/0 0.028/0/1

For the whole model, this one is composed by 4 revolute joints and 1 translational joint, as can be identified in the Figure 5.3.

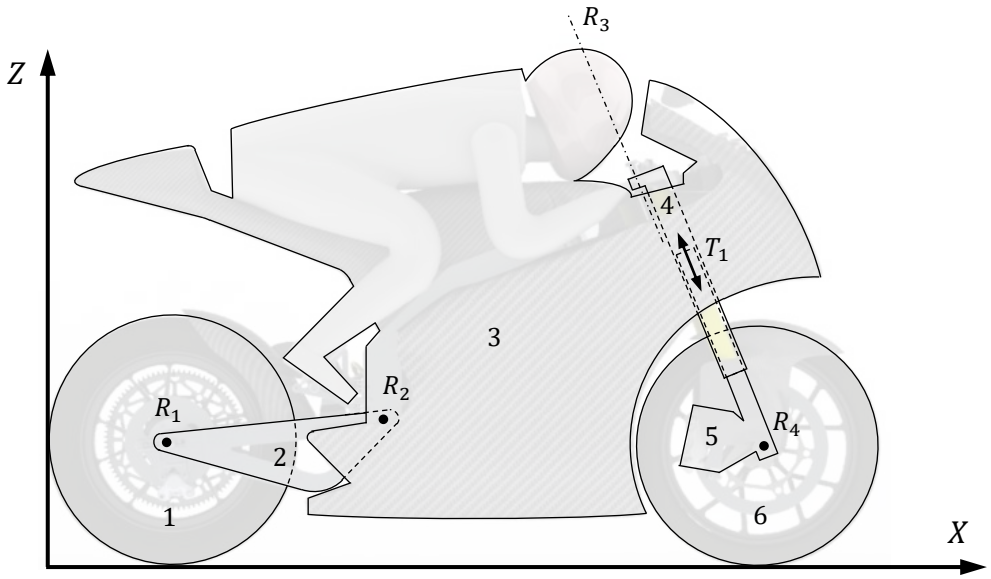

Figure 5.3: Kinematic joints location.

5.2.3 Suspension

As already mentioned, the suspension system has an important role in vehicle dynamics. The front suspension used on TLM03e is a fork telescopic, which is the most used, specially in this type of motorcycles. For the rear suspension, TLM03e is equipped with a monoshock. The rear suspension is attached to the frame and swingarm in a way called ”classic swingarm”, without connecting rod or bar linkage systems. Being both suspensions composed by a spring and a damper, the Table 5.6 gives the parameters needed to model a suspension in order to obtain suspension forces.

Table 5.6: Suspension parameters of TLM03e.

	Body i	Body j	k $[N/m]$	c $[Ns/m]$	l_0 $[m]$
Rear Suspension	2	3	180000	15000	0.310
Front Suspension	4	5	55000	1500	0.550

The stiffness coefficient k_r of the rear spring was obtained from the data sheet of the rear suspension. For the front spring, k_f is computed using Hooke's law, where the normal force in the front tire is computed from a static equilibrium. The damping coefficient c for the rear suspension is chosen to target a critically damping behaviour and for the front suspension the coefficient is based on commonly used values. Table 5.7 shows the attachment points between each rigid body for both suspensions.

Table 5.7: Suspension attachment points of TLM03e.

	Body i	Body j	$(\xi/\eta/\zeta)_i^P$ $[m]$	$(\xi/\eta/\zeta)_j^P$ $[m]$
Rear Suspension	2	3	0.152/0/0.101	-0.133/0/0.064
Front Suspension	4	5	0.0015/0/-0.005	0.028/0/-0.051

5.2.4 Tires

The slick tires used on this motorcycle are: 90/580 R17 for the front tire and 120/600 R17 for the rear tire. The nomenclature to describe the tires refers to their size, where the first number is the width in millimeters, the second is the diameter of the tire in millimeters and the third is the radius of the rim in inches. Assuming that the tire carcass radius is half of the width, the tires are modeled as follows.

Table 5.8: Tires geometry.

	Tire unloaded radius, $R_0[m]$	Carcass radius, $R_2[m]$	Toroidal radius, $R_3[m]$
Rear Tire	0.300	0.060	0.240
Front Tire	0.290	0.045	0.245

Unfortunately, it is very difficult to find the tire properties database on literature for these tire sizes. By virtue of that, the tire parameters of 180/55 presented in Chapter 4 were chosen to represent both

tires' dynamic behaviour. Of course, the tire properties do not fit with the size, causing less accurate values on simulations. However, the tire parameters found on *Adams* software database are complete and consistent with the ISO system.

5.3 Scenario 1: Straight Line

To test the tire model along with the motorcycle model, a simple straightforward trajectory was attempted. In addition to post processed graphs resulting from the simulation, *SAGA* software was used to visualize graphically the motorcycle behaviour derived from the simulation. In this software all the dynamics information of each body is uploaded as well as the files with graphic information taken from a CAD software.

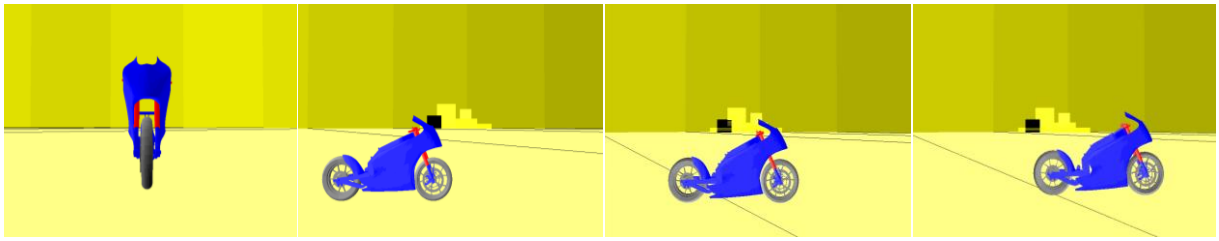

$t = 0.0\ [s]$ $t = 0.1\ [s]$ $t = 0.5\ [s]$ $t = 1.0\ [s]$

Figure 5.4: TLM03e motorcycle unassisted, for 20m/s of initial forward velocity.

Not all the bodies are represented graphically in the simulation, because some parts were to heavy to be uploaded to the software *SAGA*. The Figures 5.5, 5.6, 5.7 and 5.8 show the movement of the center of gravity of body 3 (Frame + Pilot) along with the trajectory prescribed. Although the graphs are representing the information of the body 3, they also represent directly the entire motorcycle, since body 3 is it main body.

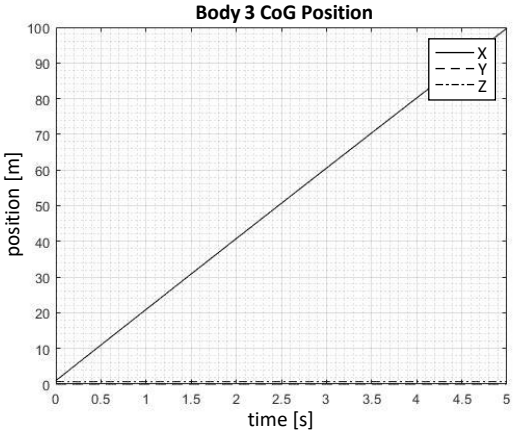

Figure 5.5: Position of body 3 along the time.

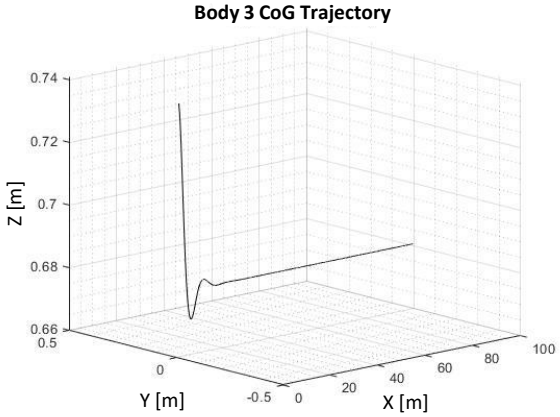

Figure 5.6: 3D trajectory of body 3.

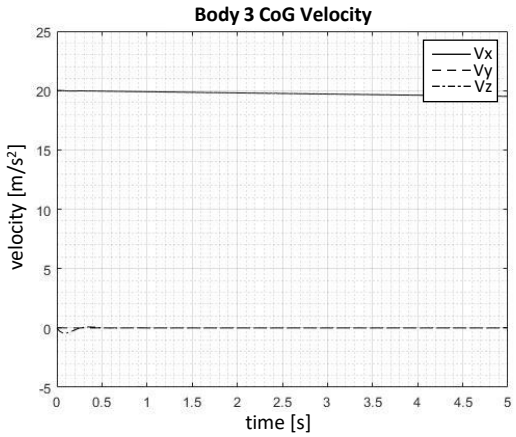

Figure 5.7: Velocity of body 3 over the three global axis.

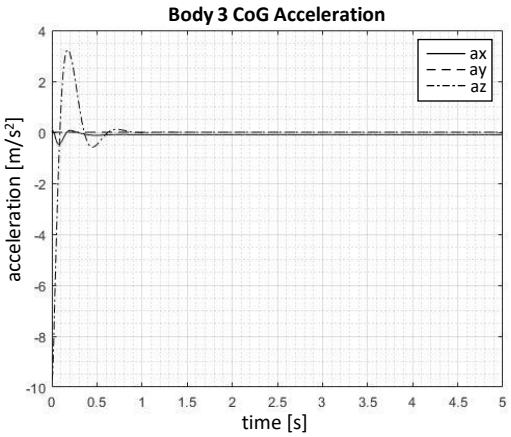

Figure 5.8: Acceleration of body 3 over the three global axis.

At the initial moment, can be observed the trajectory along Z axis of the motorcycle until stabilize (Figure 5.6). In $t = 0.0[s]$ the motorcycle is suspended very close to the ground and by the damping affect it stabilize after 1 second (Figure 5.8).

Due to the rolling resistance, the velocity decays approximately only 0.5 $[m/s]$ in 5 seconds, since no other mechanical energy dissipation is consider. Another important thing to note is that no deviation occurs along Y axis, proving that the motorcycle at this velocity is stable.

Chapter 6

Motorcycle Control

A Motorcycle is a nonlinear system and, unless it is at certain speed, it is an unstable system. Contrary to cars, motorcycles are unstable at very low speeds because forces and moments produced on the front wheel are not sufficient to self-align it. In order to stabilize the vehicle, an input from the rider is necessary. Weave and wobble effects [12] are instability effects common in motorcycle dynamics. Weave occurs at lower frequencies and wobble at higher frequencies, associated to the oscillation of the steering at higher velocities.

The control strategy used for the motorcycle is based on the work of Antos and Ambrósio [14]. In order to describe the motorcycle reduced model, the works of Marumo and Nagai [15] and Dao and Chen [16] were taking into account. The works of Yokomori et al. [18] and Marumo and Nagai [15] were consulted as options to obtain the simplified motorcycle equilibrium equations, for motorcycle motion. However, it was decided to follow the structure of the simplified motorcycle equilibrium equations presented in Marumo and Nagai [15].

In the controller design, as demonstrated by Huyge [19], a LQR controller is used for motorcycle controlling purposes. The simplicity of the reduced model idea is also discussed as a way of control over a reference line.

6.1 Description of the Motorcycle Reduced Model

The variables needed to control the motorcycle are defined in this section, recalling the particularity of the motorcycle dynamics. The simplified equations of motorcycle equilibrium are presented, based on the work by [15]. Simplifications on these equations were made in order to used a more reduced model of the motorcycle.

Although it is not the same tire model, the simplified equations of motorcycle equilibrium used in this work consider forces and moment developed on the tires.

6.1.1 State and Control Variables of a Reduced Model

The variables to represent the state of the motorcycle must be defined before describing the simplified equations for motorcycle equilibrium. As seen in Chapter 2, motorcycle needs to lean to describe a curve. Besides the state values used to monitor a car, the lean angle ϕ needs to be added to the state vector. Using a bilinear control methodology, as shown by [14] and [19], the continuous-time state-space regulator form is defined by the next equation.

$$\dot{\mathbf{z}} = \mathbf{Cz} + \mathbf{Bu} + \mathbf{Nu} \tag{6.1}$$

The state vector **z** is composed by the lateral displacement y_{ct}, angular displacement ε_{ct}, steering angle δ, lean angle ϕ and the time derivatives of each one. The variables y_{ct} and ε_{ct}, are understood as the deviations between a reference point on the motorcycle and a prescribed trajectory path.

$$\mathbf{z} = \begin{bmatrix} y_{ct} & \varepsilon_{ct} & \delta & \phi & \dot{y}_{ct} & \dot{\varepsilon}_{ct} & \dot{\delta} & \dot{\phi} \end{bmatrix}^T \tag{6.2}$$

The control vector **u** is defined by three moments applied as:

$$\mathbf{u} = \begin{bmatrix} M_h & M_{wf} & M_{wr} \end{bmatrix}^T \tag{6.3}$$

M_h is the moment applied to the handlebars in steering axis direction. The moments applied to front and rear wheel, M_{wf} and M_{wr} respectively, are braking moments or, in case of the rear wheel, can also be traction.

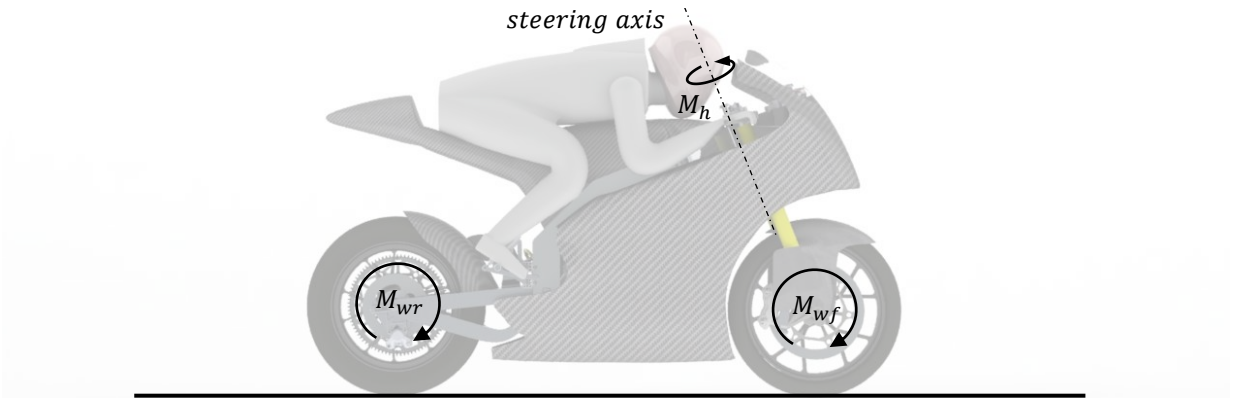

Figure 6.1: TLM03e applied moments by the control vector.

In [15] it is also presented a reduced model where it takes a different approach to motorcycles, where it is used the variables of yaw rate $\dot{\psi}$ and lateral velocity $\dot{y}_1$ to build the following state vector.

$$\mathbf{z} = \begin{bmatrix} \delta & \phi & \dot{\delta} & \dot{\phi} & \dot{y}_1 & \dot{\psi} \end{bmatrix}^T \tag{6.4}$$

But a more reduced model can be used to control a motorcycle. A motorcycle could only use the steering angle δ and the lean angle ϕ information to maintain equilibrium, as referred and used by [16] and [19]. Therefore, the state vector can be reduced to:

$$\mathbf{z} = \begin{bmatrix} \delta & \phi & \dot{\delta} & \dot{\phi} \end{bmatrix}^T \tag{6.5}$$

To control the motorcycle under a constant velocity, the moments applied on the wheels are withdrawn. For that reason, the control vector is summarized as follows:

$$\mathbf{u} = \begin{bmatrix} M_h \end{bmatrix}^T \tag{6.6}$$

The Table 6.1 shows the parameters necessary for the equilibrium equations written on the following subsections. Parameters were considered with a fix value, since very small variations occur on the motorcycle geometry after its stabilization. It was consider the default values for i_a and λ founded in [15].

Table 6.1: Values necessary for the motorcycle equilibrium equations.

Symbol	Value	Units	Description
g	9.81	$[m/s^2]$	Gravity
M_f	22.05	$[kg]$	Front fork system mass
M_r	201.10	$[kg]$	Main frame mass
I_{fx}	2.10	$[kg\,m^2]$	Moment of inertia of front fork around x
I_{fz}	0.27	$[kg\,m^2]$	Moment of inertia of front fork around z
I_{rx}	16.87	$[kg\,m^2]$	Moment of inertia of main frame around x
I_{rz}	19.04	$[kg\,m^2]$	Moment of inertia of main frame around z
i_{fy}	0.19	$[kg\,m^2]$	Moment of inertia of front wheel
i_{ry}	0.35	$[kg\,m^2]$	Moment of inertia of rear wheel
i_a	0.902	$[kg\,m^2]$	Polar moment of inertia of engine flywheel
λ	1.0	–	Gear ratio between rear wheel and engine flywheel
e	0.026	$[m]$	Distance from front fork CoG to steering axis
j_a	0.620	$[m]$	Height of front fork CoG
k	0.653	$[m]$	Distance from front fork CoG to main frame CoG
t	0.086	$[m]$	Normal trail
h	0.668	$[m]$	Height of main frame CoG
l_1	0.765	$[m]$	Longitudinal distance from front wheel center to main frame CoG
l_2	0.640	$[m]$	Longitudinal distance from rear wheel center to main frame CoG
h'	0.650	$[m]$	Height of whole motorcycle CoG
l'	0.064	$[m]$	Longitudinal distance from main frame CoG to whole motorcycle CoG
R_f	0.290	$[m]$	Radius of front wheel
R_r	0.300	$[m]$	Radius of rear wheel
τ	0.40	$[rad]$	Caster angle
C_δ	20	$[Nm\,s/rad]$	Steering damper coefficient
Z_f	-1.097	$[kN]$	Vertical load acting on front wheel
Z_r	-1.092	$[kN]$	Vertical load acting on rear wheel

The steering constraint developed in Chapter 3 is used to monitor the angle of the steering. However, it is important not to confuse the angle of the wheel steered δ_f on the road plane and the steering angle δ given by the handlebars position. This angles are related with function of the rake angle τ of the motorcycle.

$$\delta_f = \delta \cos(\tau) \tag{6.7}$$

Figure 6.2 shows the angles described in equation 6.7 to better understanding the relation between them.

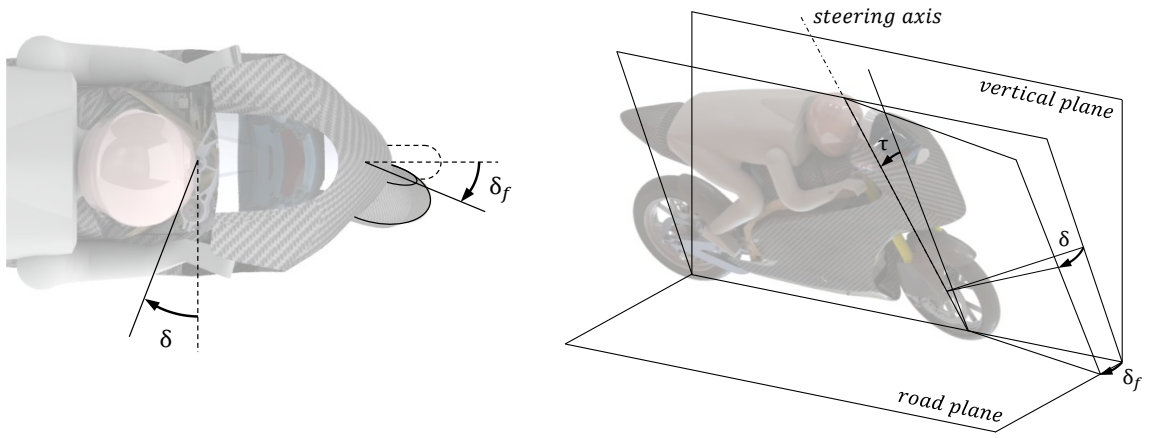

(a) Top view. (b) Perspective view.

Figure 6.2: Motorcycle relation between steering angle and angle of the front wheel steered.

Beyond the parameters presented on Table 6.1, a set of values are used to represent the forces Y and moments T acting on the tires that are considered in the simplified equations of motorcycle equilibrium. The values depend on normal forces of rear and front tire, Z_f and Z_r respectively. In Appendix C can be found the relation to obtain the Y and T values. Although the tire model is not the Pacejka tire model, it adds robustness to the simplified equations of motorcycle equilibrium. The term v existing on the following equations corresponds to the motorcycle forward velocity.

6.1.2 Lateral Motion

The lateral motion corresponds to the lateral velocity of the motorcycle and can be described through the following expression.

$$\ddot{y}_1 = \left[-M_f\, k\ddot{\psi} - \left(M_f + M_r\right) v\dot{\psi} + \left(M_f\, j_a + M_r h\right)\ddot{\phi} + M_f\, e\ddot{\delta} - Y_f - Yr\right] \frac{1}{Mf + Mr} \tag{6.8}$$

Developing the expression and cutting the terms not necessary for control, it follows:

$$\begin{aligned}\ddot{y}_1 = \Bigg[& \left\{ \left(M_f + M_r\right) v + C_{YS1}\frac{1}{v} l_1 - C_{YS2}\frac{1}{v} l_2 \right\} \dot{\psi} + \left(C_{YS1}\frac{1}{v} + C_{YS2}\frac{1}{v} \right) \dot{y}_1 + \left(-C_{YS1} t \frac{1}{v} \right) \dot{\delta} \\ & + \left(-C_{YS1}\cos\tau - C_{YC1}\sin\tau \right) \delta + \left(-C_{YC1} + C_{YC2} \right) \phi \Bigg] \frac{1}{M_f + M_r}\end{aligned} \tag{6.9}$$

6.1.3 Yawing motion

The yawing motion, which is the angular motion around yaw axis, can be described as follows:

$$\begin{aligned}\ddot{\psi} = \Bigg[& - M_h \cos\tau - M_f k \ddot{y}_1 - M_f k v \dot{\psi} - \left\{ M_f j_a k + \left(I_{fz} - I_{fx} \right) \sin\tau\cos\tau \right\} \ddot{\phi} + \left(\frac{i_{fy}}{R_f} + \frac{i_{ry} + i_a \lambda}{R_r} \right) v \dot{\phi} \\ & - \left(M_f e k + I_{fz}\cos\tau \right) \ddot{\delta} + \left(\frac{i_{fy}}{R_f} v \sin\tau \right) \dot{\delta} + l_1 Y_f - l_2 Y_r + T_{zf} + T_{zr} \Bigg] \frac{1}{y_y}\end{aligned} \tag{6.10}$$

where y_y is given by,

$$y_y = M_f k^2 + I_{fx}\sin^2\tau + I_{fz}\cos^2\tau + I_{rz} \tag{6.11}$$

Developing the terms of the tire forces and moments, and cutting the terms not necessary for the control, it follows:

$$\begin{aligned}\ddot{\psi} = \Bigg[& M_h \cos\tau + \left(-M_f k v - l_1^2 C_{YS1}\frac{1}{v} - l_2^2 C_{YS2}\frac{1}{v} - C_{ZS1}\frac{1}{v} l_1 + C_{ZS2}\frac{1}{v} l_2 \right) \dot{\psi} \\ & + \left(\frac{i_{fy}}{R_f} + \frac{i_{ry} + i_a \lambda}{R_r} \right) v \dot{\phi} + \left(\frac{i_{fy}}{R_f} v \sin\tau + C_{YS1}\frac{1}{v} l_1 t + C_{ZS1}\frac{1}{v} t \right) \dot{\delta} \\ & + \left(-C_{YS1}\frac{1}{v} l_1 + C_{YS2}\frac{1}{v} l_2 - C_{ZS1}\frac{1}{v} - C_{ZS2}\frac{1}{v} \right) \dot{y}_1 + \left(C_{YS1}\cos\tau l_1 + C_{YC1}\sin\tau l_1 \right. \\ & \left. + C_{ZS1}\cos\tau + C_{ZC1}\sin\tau \right) \delta + \left(C_{YC1} l_1 - C_{YC2} l_2 + C_{zc1} + C_{ZC2} \right) \phi \Bigg] \frac{1}{y_y}\end{aligned} \tag{6.12}$$

6.1.4 Steering Motion

The steering motion, which is around the steering axis, is represented by the following equation. Note that equation 6.13 will be developed until reaching the final expression that will be used on the controller.

$$\begin{aligned}\ddot{\delta} = \Bigg[& - M_f e \ddot{y}_1 - \left(M_f e k + I_{fz}\cos\tau \right) \ddot{\psi} - \left(M_f e + \frac{i_{fy}}{R_f}\sin\tau \right) v \dot{\psi} - \left(M_f e j_a + I_{fz}\sin\tau \right) \ddot{\phi} \\ & + \frac{i_{fy}}{R_f}\cos\tau v \dot{\phi} - \left(t Z_f - M_f e g \right) \phi - C_\delta \dot{\delta} - \left(t Z_f - M_f e g \right) \sin\tau\delta - t Y_f + T_{zf}\cos\tau + T_{xf}\sin\tau + M_h \Bigg] \frac{1}{s_s}\end{aligned} \tag{6.13}$$

where s_s is given by,

$$s_s = M_f e^2 + I_{fz} \tag{6.14}$$

Developing the terms of the tire forces and moments, and cutting the terms not necessary for the control, it follows:

$$\begin{aligned}\ddot{\delta} = \Bigg[& \left\{ -\left(M_f e + \frac{i_{fy}}{R_f} \right) v + C_{YC1} \frac{1}{v} t l_1 - C_{ZS1} \frac{1}{v} l_1 \cos\tau - C_{XS1} \frac{1}{v} l_1 \sin\tau \right\} \dot{\psi} + \left(\frac{i_{fy}}{R_f} \cos\tau v \right) \dot{\phi} \\ & + \left\{ -\left(t Z_f - M_f e g \right) - C_{YC1} t + C_{ZC1} \cos\tau + C_{XC1} \sin\tau \right\} \phi \\ & + \left\{ -C_\delta - C_{YS1} \frac{1}{v} t^2 + C_{ZS1} \frac{1}{v} t \cos\tau + C_{XS1} \frac{1}{v} t \sin\tau \right\} \dot{\delta} + \left\{ -\left(t Z_f + M_f e g \right) \sin\tau \right. \\ & - C_{YS1} t \cos\tau - C_{YC1} t \sin\tau + C_{ZS1} \cos^2\tau + C_{ZC1} \cos\tau \sin\tau + C_{XS1} \cos\tau \sin\tau \\ & \left. + C_{XC1} \sin^2\tau \right\} \delta + \left\{ C_{YS1} \frac{1}{v} t - C_{ZS1} \frac{1}{v} \cos\tau - C_{XS1} \frac{1}{v} \sin\tau \right\} \dot{y}_1 + M_h \Bigg] \frac{1}{s_s} \end{aligned} \tag{6.15}$$

To be used on the very reduced model, the expression can be simplified, cutting the terms that will not compose the **C** matrix. Only the terms corresponding to the state vector of the equation 6.5 remain.

$$\begin{aligned}\ddot{\delta} = \Bigg[& \left(\frac{i_{fy}}{R_f} \cos\tau v \right) \dot{\phi} + \left\{ -\left(t Z_f - M_f e g \right) - C_{YC1} t + C_{ZC1} \cos\tau + C_{XC1} \sin\tau \right\} \phi \\ & + \left\{ -C_\delta - C_{YS1} \frac{1}{v} t^2 + C_{ZS1} \frac{1}{v} t \cos\tau + C_{XS1} \frac{1}{v} t \sin\tau \right\} \dot{\delta} + \left\{ -\left(t Z_f + M_f e g \right) \sin\tau \right. \\ & - C_{YS1} t \cos\tau - C_{YC1} t \sin\tau + C_{ZS1} \cos^2\tau + C_{ZC1} \cos\tau \sin\tau + C_{XS1} \cos\tau \sin\tau \\ & \left. + C_{XC1} \sin^2\tau \right\} \delta + M_h \Bigg] \frac{1}{s_s} \end{aligned} \tag{6.16}$$

6.1.5 Rolling Motion

Equation 6.17 reveals the motorcycle motion around X axis. This equation is also regrouped with the correct terms to be used on the controller.

$$\begin{aligned}\ddot{\phi} = \Bigg[& - M_h \sin\tau - \left(M_f j_a + M_r h \right) \ddot{y}_1 - \left\{ M_f j_a k + \left(I_{fz} - I_{fx} \right) \sin\tau \cos\tau \right\} \ddot{\psi} \\ & - \left\{ M_f j_a + M_r h + \frac{i_{fy}}{R_f} + \frac{i_{ry} + i_a \lambda}{R_r} \right\} v \dot{\psi} + \left(M_r j_a + M_r h \right) g \phi - \left(M_f e j_a + I_{fz} \sin\tau \right) \ddot{\delta} \\ & - \left(\frac{i_{fy}}{R_f} \cos\tau \right) v \dot{\delta} - \left(t Z_f - M_f e g \right) \delta + T_{xf} + T_{xr} \Bigg] \frac{1}{r_r} \end{aligned} \tag{6.17}$$

where r_r is given by,

$$r_r = M_f j_a^2 + M_r h^2 + I_{fx} \cos^2\tau + I_{fz} \sin^2\tau + I_{rx} \tag{6.18}$$

Developing the terms of the tire forces and moments, and cutting the terms not necessary for the control, it follows:

$$\begin{aligned}\ddot{\phi} = \Bigg[& - M_h \sin\tau + \left\{ -\left(M_f j_a + M_r h + \frac{i_{fy}}{R_f} + \frac{i_{ry} + i_a \lambda}{R_r} \right) v - C_{XS1} \frac{1}{v} l_1 + C_{XS2} \frac{1}{v} l_2 \right\} \dot{\psi} \\ & + \left\{ \left(M_f j_a + M_r h \right) g + C_{XC1} + C_{XC2} \right\} \phi + \left\{ -\frac{i_{fy}}{R_f} \cos\tau v + C_{XS1} \frac{1}{v} t \right\} \dot{\delta} \\ & + \left\{ -\left(t Z_f - M_f e g \right) + C_{XS1} \cos\tau + C_{XC1} \sin\tau \right\} \delta + \left(-C_{XS1} \frac{1}{v} - C_{XS2} \frac{1}{v} \right) \dot{y}_1 \Bigg] \frac{1}{r_r} \end{aligned} \tag{6.19}$$

As was done in equation 6.16, the following equation only has the terms corresponding to the state vector 6.5 used to construct the matrix **C**.

$$\begin{aligned}\ddot{\phi} = &\Bigg[- M_h \sin\tau + \left\{\left(M_f j_a + M_r h\right) g + C_{XC1} + C_{XC2}\right\}\phi + \left\{-\frac{i_{fy}}{R_f}\cos\tau v + C_{XS1}\frac{1}{v}t\right\}\dot{\delta} \\ &+ \left\{-\left(tZ_f - M_f eg\right) + C_{XS1}\cos\tau + C_{XC1}\sin\tau\right\}\delta\Bigg]\frac{1}{r_r}\end{aligned} \tag{6.20}$$

6.1.6 Continuous-Time Space-State Description

As defined before, continuous-time space-state expression takes the form:

$$\dot{\mathbf{z}} = \mathbf{Cz} + \mathbf{Bu} + \mathbf{Nu} \tag{6.21}$$

where state vector $\mathbf{z} \in \Re^n$:

$$\mathbf{z} = \begin{bmatrix}\phi & \theta & \dot{\phi} & \dot{\theta}\end{bmatrix}^T \tag{6.22}$$

and the control vector $\mathbf{u} \in \Re^m$ as follows:

$$\mathbf{u} = \begin{bmatrix}M_h\end{bmatrix}^T \tag{6.23}$$

The matrices **C**, **B** and **N** are achieved from the terms resultants of equations 6.16 and 6.20. The matrix **C** is composed by three submatrices, due to the fact that matrix **C** has large matrix entries.

$$\mathbf{C} = \begin{bmatrix}\mathbf{C}_1 & \mathbf{C}_2 & \mathbf{C}_3\end{bmatrix} \tag{6.24}$$

where,

$$\mathbf{C}_1(1,1) = \mathbf{C}_1(2,1) = 0 \tag{6.25}$$

$$\begin{aligned}\mathbf{C}_1(3,1) = &\left\{-\left(t_{Zf} + M_f eg\right)\sin\tau - C_{YS1}t\cos\tau - C_{YC1}t\sin\tau + C_{ZS1}\cos^2\tau\right. \\ &\left.+C_{ZC1}\cos\tau\sin\tau + C_{XS1}\cos\tau\sin\tau + C_{XC1}\sin^2\tau\right\}\frac{1}{ss}\end{aligned} \tag{6.26}$$

$$\mathbf{C}_1(4,1) = \left\{-\left(t_{Zf} + M_f eg\right) + C_{XS1}\cos\tau + C_{XC1}\sin\tau\right\}\frac{1}{ff} \tag{6.27}$$

$$\mathbf{C}_2 = \begin{bmatrix} 0 \\ 0 \\ \left\{-\left(t_{Zf} + M_f eg\right) - C_{YC1}t + C_{ZC1}\cos\tau + C_{XC1}\sin\tau\right\}\frac{1}{ss} \\ \left\{\left(M_f j_a + M_r h\right) g + C_{XC1} + C_{XC2}\right\}\frac{1}{ff}\end{bmatrix} \tag{6.28}$$

$$\mathbf{C}_3 = \begin{bmatrix} 1 & 0 \\ 0 & 1 \\ \left(-C_\delta - C_{YS1}\frac{1}{v}t^2 + C_{ZS1}\frac{1}{v}t\cos\tau + C_{XS1}\frac{1}{v}t\sin\tau\right)\frac{1}{ss} & \left(\frac{i_{fy}}{R_f}v\cos\tau\right)\frac{1}{ss} \\ \left(-\frac{i_{ft}}{R_f}v\cos\tau + C_{XS1}\frac{1}{v}t\right)\frac{1}{ff} & 0\end{bmatrix} \tag{6.29}$$

$$\mathbf{B} = \begin{bmatrix} 0 \\ 0 \\ \frac{1}{M_f e + I_{fz}} \\ -\sin\tau \frac{1}{f f} \end{bmatrix} \tag{6.30}$$

$$\mathbf{N} = \mathbf{N}_\phi = \begin{bmatrix} 0 \\ 0 \\ 0 \\ 0 \end{bmatrix} \tag{6.31}$$

6.2 Design of the Controller

The job of a rider in a motorcycle is to travel through a predefined route without losing the control of the vehicle. Keeping this idea in mind, the controller takes for instance the place of the rider in the work of motorcycle stabilization, known as virtual driver.

6.2.1 Description of the Controller

Using a controller based on the methodology proposed by [13] and used by [19] for bilinear control, the continuous-time state-space regulator is presented as:

$$\dot{\mathbf{z}} = \mathbf{C}\mathbf{z} + \mathbf{B}\mathbf{u} + \mathbf{N}\mathbf{u} \tag{6.32}$$

Matrix $\mathbf{N} \in \Re^{n \times m}$ represents the sum of product of state variables by $\mathbf{N}_j$ matrices. In this case $o = 1$ with $z_1 = \phi$ and $\mathbf{N}_1 = \mathbf{N}_\phi$, however $\mathbf{N}_\phi$ is null.

$$\mathbf{N} \equiv \sum_{j=1}^{o} z_j \mathbf{N}_j \tag{6.33}$$

Initial values for $\mathbf{z}$ are needed to initialize the controller model.

$$\mathbf{z}(0) = \mathbf{z}_0 \tag{6.34}$$

The state vector $\mathbf{z} \in \Re^n$ and the control vector $\mathbf{u} \in \Re^{n \times m}$, are related by the state-feedback law:

$$\mathbf{u} = -\mathbf{K}_{FB}(\mathbf{z})\mathbf{z} \tag{6.35}$$

where the optimal gain matrix $\mathbf{K}_{FB} \in \Re^{n \times m}$ is defined in a way that equation 6.35 minimizes the quadratic performance index J.

$$J = \frac{1}{2} \int_{t_0}^{t_\infty} (\mathbf{z}^T \mathbf{Q}\mathbf{z} + \mathbf{u}^T \mathbf{R}\mathbf{u}) dt \tag{6.36}$$

The symmetric weighting matrices $\mathbf{Q} \in \Re^{n \times m}$ and $\mathbf{R} \in \Re^{n \times m}$ are positive semi-definite and definite matrices, respectively. Notice the values of matrices $\mathbf{Q}$ and $\mathbf{R}$ are set by the user and they have a major influence on the behaviour of the controller. In this work, $\mathbf{Q}$ and $\mathbf{R}$ are diagonal matrices.

The calculation of the optimal gain $\mathbf{K}_{FB}$ is done by solving the state-dependent form of the algebraic Riccati equation:

$$\mathbf{C}^T\mathbf{S}(\mathbf{z}) + \mathbf{S}(\mathbf{z})\mathbf{C} - \mathbf{S}(\mathbf{z})(\mathbf{B}+\mathbf{N})\mathbf{R}^{-1}(\mathbf{B}+\mathbf{N})^T\mathbf{S}(\mathbf{z}) + \mathbf{Q} = 0 \tag{6.37}$$

Where the solution of equation 6.37 are obtained using the relation between $\mathbf{S}(\mathbf{z})$ and the optimal gain:

$$\mathbf{K}_{FB} = \mathbf{R}^{-1}(\mathbf{B}+\mathbf{N})^T\mathbf{S}(\mathbf{z}) \tag{6.38}$$

The following assumptions need to be verified in order to use this approach:

1. The differential equation 6.32 has a solution defined on $[0, +\infty[$ for each admissible input $\mathbf{u}$ and $\mathbf{z}(t) \to 0$ as $t \to 0$;
2. The pair $(\mathbf{C}, \mathbf{B}+\mathbf{N})$ is stabilized in the linear system for all $\mathbf{z} \in \Re^n$;
3. The full state vector $\mathbf{z}$ is available for use in the control law.

The function lqr of Matlab software is used to obtained the solution of the Ricatti equation from which the gain matrix $\mathbf{K}_{FB}$ is calculated.

6.2.2 Implementation

The motorcycle controller structure is very similar to the one presented by [14] and implemented by [19]. This work focuses more on [19] as it treats the controller model to reflect the motorcycle dynamics.

The controller module is processed on the dynamics multibody program in the function *Force*, where all the forces acting on the system are calculated in order to obtain the $\mathbf{g}$ forces vector. Although the chosen output of the controller not being a force (handlebars moment M_h), this is when it is known the position, velocity and acceleration of the steering angle δ to fill in the constraint matrices before solving the system of the equation of motion, defined by the process *Solve* presented in the flowchart of Figure 3.5.

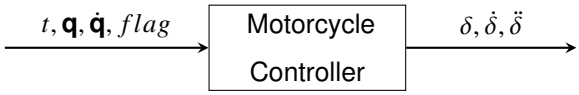

Figure 6.3: Controller module.

Figure 6.3 shows the input and output of the motorcycle controller. The input variables are: the time t, the position vector $\mathbf{q}$ and the velocity vector $\dot{\mathbf{q}}$ of body 3 (Frame + Pilot), and a $flag$ value. For the output variables: the position δ, velocity $\dot{\delta}$ and acceleration $\ddot{\delta}$ of the steering angle.

The controller algorithm is divided into two phases. The initialization ($flag = 2$), which happens at the beginning for $t = 0$, and for every time step ($flag = 1$) during the motorcycle motion. The list below describes the steps that takes place in the algorithm.

Initialization:

Step 1: Initialise the variables given in table 6.1 and weighting matrices **Q** and **R** in equation 6.36;

Step 2: Initialize the steering dynamics by defining $\delta = \delta(0)$ and $\dot{\delta} = \dot{\delta}(0)$;

For every time step:

Step 3: Calculate the forward velocity v from $\dot{\mathbf{q}}$;

Step 4: Determine the actual roll angle ϕ_M of the main frame using equation 6.39;

Step 5: For $flag = 1$, integrates δ and $\dot{\delta}$ from the previous time step using Adams-Bashforth algorithm;

Step 6: Determination of the state vector **z** of equation 6.22;

Step 7: Construct the matrices **C**, **B** and **N** from equations 6.24 through 6.33;

Step 8: Calculate the optimal gain $\mathbf{K}_{FB}$ using equation 6.38 and evaluate the control vector **u** by using equation 6.35;

Step 9: Evaluate the time derivative of the state-variable $\dot{\mathbf{z}}$ by using equation 6.32;

Step 10: Exit *Controller* function and returns to the dynamics analysis program with the new steering angle and its time derivatives δ, $\dot{\delta}$ and $\ddot{\delta}$;

Equation 6.39 computes the roll angle ϕ_M, where is used the entry of the transformation matrix $\mathbf{A}_3(3,2)$ corresponding to the rigid body $i = 3$ (Frame + Pilot).

$$\phi_M = \arccos(-\mathbf{A}_3(3,2)) - \frac{\pi}{2} \tag{6.39}$$

As known, the LQR control tries to minimize a cost function, leading to the variables of the state vector become as small as possible. Attending to this, the roll angle ϕ of the state vector **z**, is given by the difference of the actual roll angle ϕ_M and a desired roll angle ϕ_{des}.

$$\phi = \phi_M - \phi_{des} \tag{6.40}$$

6.3 Prescribe a Trajectory

In this section the controller is used to maneuver the motorcycle in order to describe a curve with constant radius and a curve counter curve. Modification of some parameters that influence the control are explained below. For all the scenarios, the road is defined as being horizontal. A simple method is attempted in order to follow a reference line, without adding variables to the state vector presented.

6.3.1 Scenario 2: Curve

Curving in a constant radius curve is the simpler scenario to demonstrate the capability of the motorcycle controller. Starting at $v = 20m/s$, it was defined a desired roll angle of $\phi_{des} = 0.5[rad]$ at $t = 0.6[s]$, where at this time the motorcycle is practically damped. Figure 6.4 shows two time steps, being the first time step taken before $t = 0.6[s]$ and the second at $t = 0.6$ when the steering constraints are applied in order to achieve the desired roll angle.

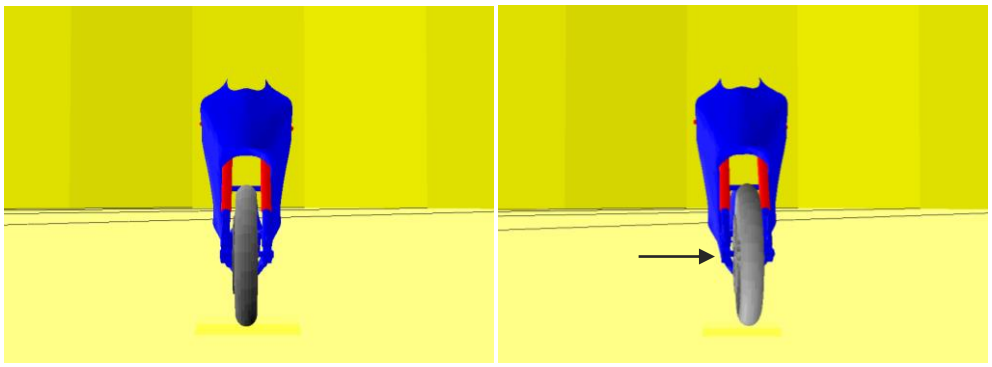

Figure 6.4: Counter steering application to starting turning.

In the second time step, it can be verified the peculiar movement taken by the steering and, consequently, of the front wheel. As described in Chapter 2, a counter steering is firstly applied to the steering to turn the motorcycle. Figure 6.4 shows the front wheel movement to the left before the motorcycle goes to the right (pilot perspective), since the desired angle is positive.

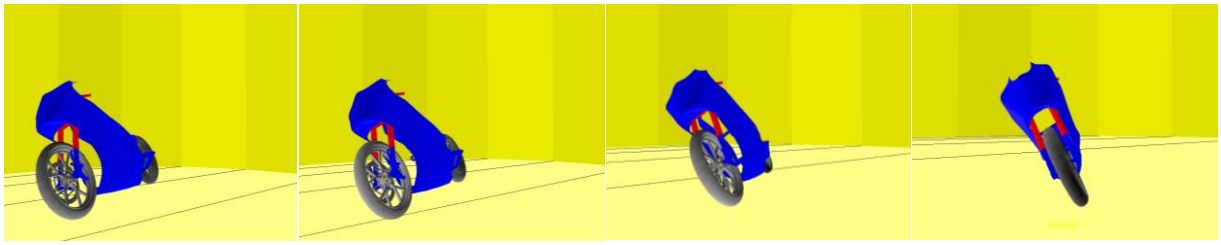

$t = 2.0\ [s]$ $t = 1.5\ [s]$ $t = 1.0\ [s]$ $t = 0.7\ [s]$

Figure 6.5: Time steps in curve scenario.

In order to accomplish this curving scenario, some modification were made. As identified by [19], the entry $\mathbf{C}(4,1)$ of the matrix $\mathbf{C}$ is responsible for the steering angle's interaction with the leaning angle. Better results were achieved by setting the matrix entry $\mathbf{C}(4,1) = -80$. Modifications to the weighting matrix $\mathbf{Q}$ were necessary, leading to more weight to the steering position.

$$\mathbf{Q}_{diag} = \begin{bmatrix} 100 & 1 & 1 & 1 \end{bmatrix} \tag{6.41}$$

$$\mathbf{R} = \begin{bmatrix} 1 \end{bmatrix} \tag{6.42}$$

In Figures 6.6 to 6.9 can be visualize the evolution of the state vector **z** and the control vector **u**.

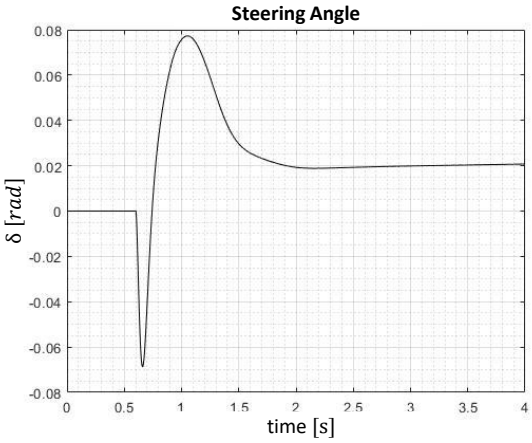

Figure 6.6: Steering angle δ over the time.

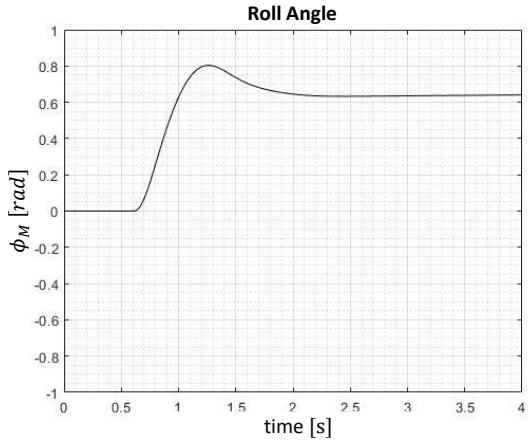

Figure 6.7: Roll angle ϕ_M over the time.

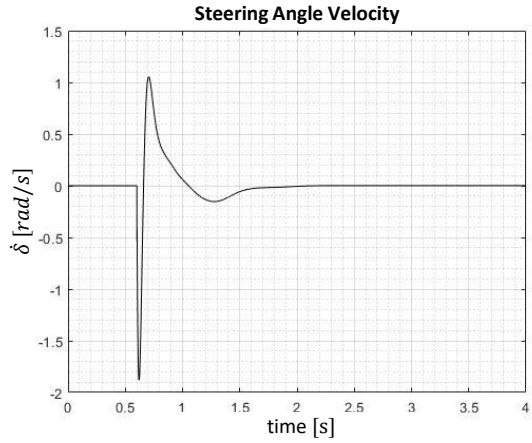

Figure 6.8: Steering angle velocity $\dot{\delta}$ over the time.

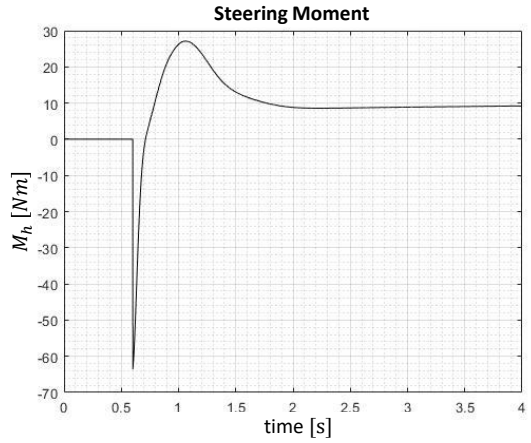

Figure 6.9: Moment M_h applied to the steering over the time.

It can be observed a smooth transition until the stabilization of the roll angle, however exist overshoot. The final roll angle also presents a relative error about 20% higher than the expected, possible derived from the combination of values: coefficient $\mathbf{C}(4,1)$, matrices **Q** and **R**. It was observed, when the coefficient approaches 0, the error in the final roll angle gets very small but the overshoot increases significantly, leading sometimes to an instability. When the coefficient becomes more negative, the opposite happens. In initial simulations, it was verified an oscillation of the steering. To resolve that, the steering damper coefficient was set to $C_\delta = 20[Nms/rad]$.

Figure 6.10 shows the trajectory prescribed by the motorcycle in the plane XY, where the curve scenario can be identified. In Figure 6.11 can be visualize a decrease in velocity Vx and an increase in velocity Vy in absolute value, describing the velocity in a curve.

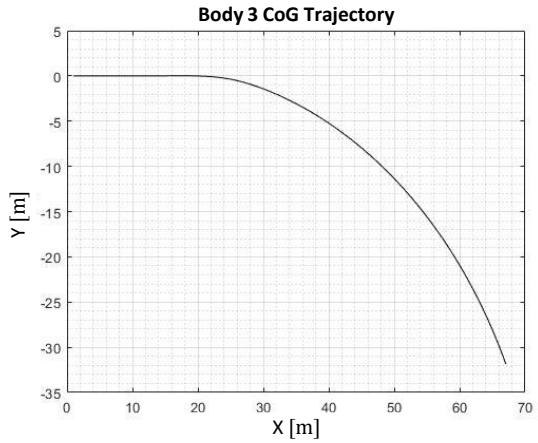

Figure 6.10: Trajectory on the plane XY.

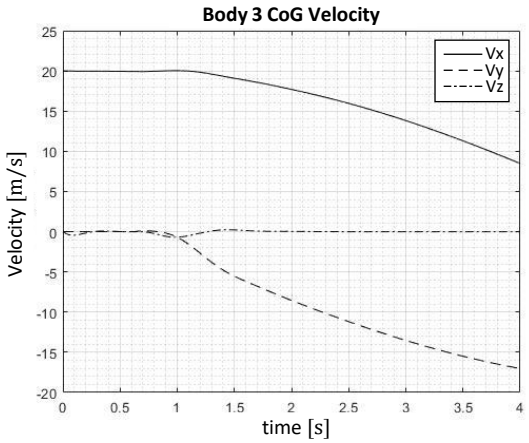

Figure 6.11: Velocity Vx, Vy and Vz over time.

6.3.2 Scenario 3: Curve Counter Curve

Curve counter curve, or curve in S shape, raise other challenges for the motorcycle controller. In this scenario, the motorcycle change the roll angle from $\phi_{des} = 0.5[rad]$ to $\phi_{des} = -0.5[rad]$ almost in an instant. Also starting with $v = 20[m/s]$, it was defined a roll angle $\phi_{des} = 0.5[rad]$ at $t = 0.6[s]$ and a desired roll angle $\phi_{des} = -0.5[rad]$ at $t = 3.5[s]$.

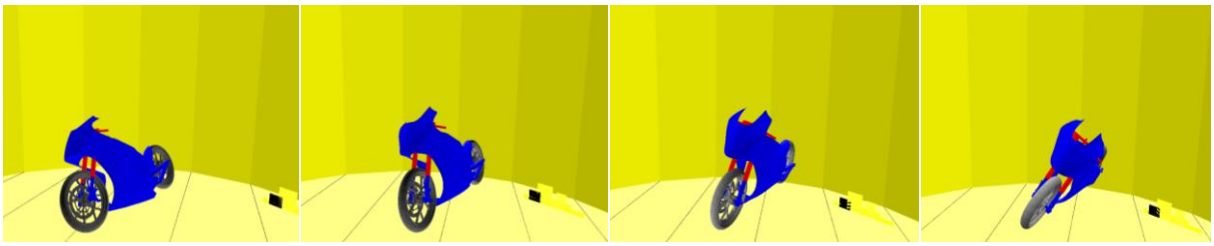

$t = 3.5\ [s]$ $t = 4.1\ [s]$ $t = 4.2\ [s]$ $t = 5.2\ [s]$

Figure 6.12: Time steps in curve counter curve scenario.

Also for this scenario, the values of $\mathbf{C}(4,1) = -80$ was maintained as well as the values of the matrices **Q** and **R**. The steering damper coefficient $C_\delta = 20[Nms/rad]$ also remains unchanged.

$$\mathbf{Q}_{diag} = \begin{bmatrix} 100 & 1 & 1 & 1 \end{bmatrix} \tag{6.43}$$

$$\mathbf{R} = \begin{bmatrix} 1 \end{bmatrix} \tag{6.44}$$

In Figures 6.13 to 6.16 can be visualize the evolution of the state vector **z** and the control vector **u**.

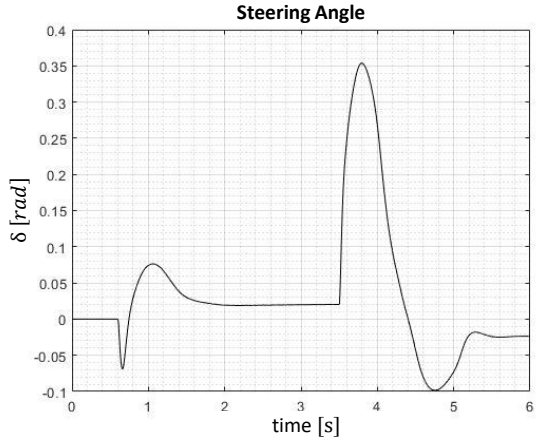

Figure 6.13: Steering angle δ over the time.

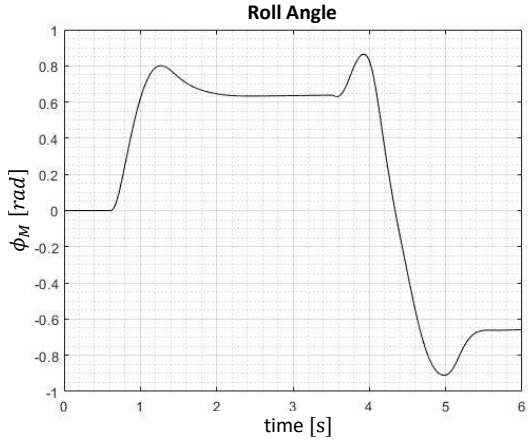

Figure 6.14: Roll angle ϕ_M over the time.

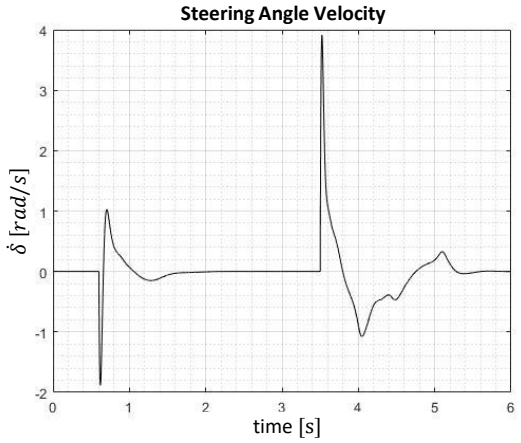

Figure 6.15: Steering angle velocity $\dot{\delta}$ over the time.

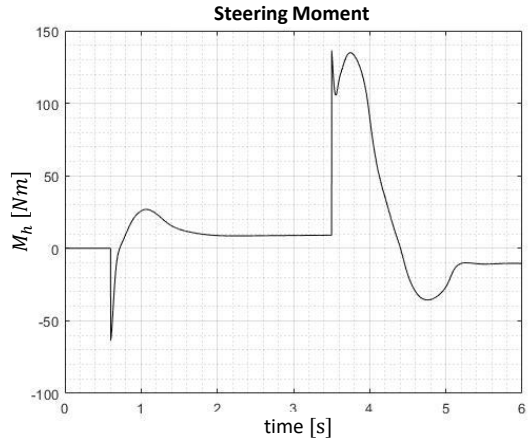

Figure 6.16: Moment M_h applied to the steering over the time.

In the transition of roll angle values at $t = 3.5[s]$, as expected, the overshoot value is more salient. The error of the roll angle is the same (about 20% higher than the expected), even to the left side, after the stabilization of the motorcycle.

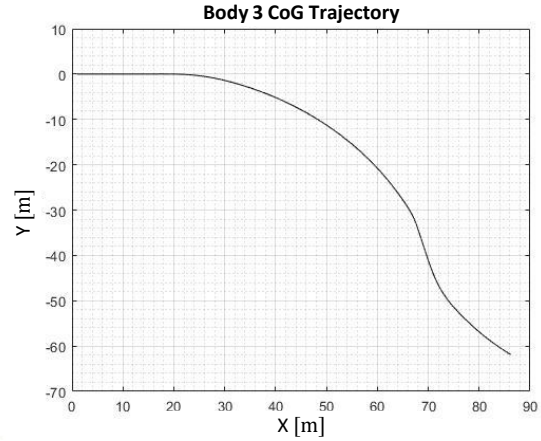

Figure 6.17: Trajectory on the plane XY.

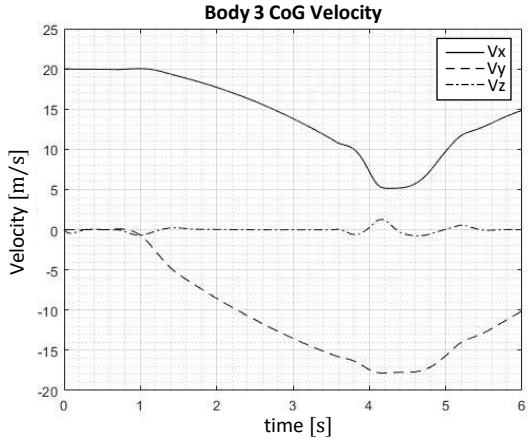

Figure 6.18: Velocity Vx, Vy and Vz over time.

The left graph above shows the trajectory prescribed by the motorcycle in the plane XY, where the curve counter curve scenario can be identified. The graph on the right shows a decrease in velocity Vx and an increase in velocity Vy in absolute value up to time $t = 4.5[s]$, then it reverses.

6.3.3 Scenario 4: Reference Line

Although the efforts made to reduce the error in the roll angle, the control system revealed an ineffectiveness in matching the desired roll angle. Thus, not improving the efficiency of the controller, a factor of 0.8 was applied to the desired roll angle ϕ_{des} so that the control output relative error is compensated. With this, it is possible to demonstrate scenario 4 where the motorcycle follow a reference line.

In an attempt to describe a trajectory following a reference line, a simple trajectory was constructed as shown in Figure 6.19. The reference line was defined by adding three segments, where each segments is determined by its segment length l_c and radius of curvature R_c, as describe in Table 6.2.

Table 6.2: Reference line properties.

Segment number n	Radius of curvature $R_c[m]$	Segment length $l_c[m]$
1	0	20
2	60	45
3	-80	100

The reduced model used in this work, does not include the state variables necessary to follow explicitly a reference line, such as the lateral displacement y_{ct}, the angular displacement ε_{ct} and its time derivatives. These variables are responsible for forcing the vehicle to follow a reference line, as demonstrated in [14]. A different method can be used to give implicitly the information of the reference line to one of the state variables used in this work. As referred in Chapter 2, a steady state cornering in plane is described by the centrifugal forces F_c actuated on the motorcycle and its weight W. Considering the motorcycle in steady state cornering, the roll angle necessary to follow the reference line is accomplished by:

$$\phi_{des} = \arctan\left(\frac{F_c}{W}\right) = \arctan\left(\frac{M\frac{v_x^2}{R_c}}{Mg}\right) \tag{6.45}$$

where v_x is the forward velocity, M the total mass and g the gravity acceleration.

Performing the simulation with the computation of the desired roll angle ϕ_{des}, the Figure 6.19 distinguished the reference line constructed and the trajectory done by the motorcycle. The reference point used in the motorcycle is the CoG of the body 3.

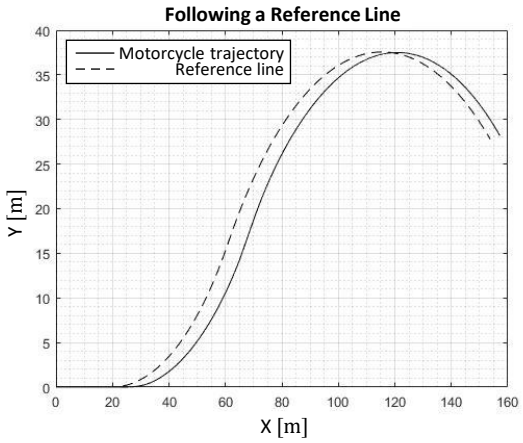

Figure 6.19: Motorcycle trajectory in an attempt to follow the reference line.

As first analysis, Figure 6.19 show that the shape of the reference line and the motorcycle trajectory are almost coincidental, demonstrating that equation 6.45 performs very well even it is used for steady state cornering.

The results on Figure 6.19 also show a relevant deviation of the trajectory performed by the motorcycle from the reference line, as expected. This happens by the fact that the response of the controller to making turn the motorcycle is very delayed. An approach used to this problem is called by distance preview, where the controller anticipates the necessity of turning in order to describe the trajectory [20]. This strategy, also referred in [16], gives the necessary distance preview, to target a point in the reference line for the controller act in time. Normally, the distance preview L_{pre} is defined as the product of the forward velocity v_x and a regulated time preview T_{pre}:

$$L_{pre} = v_x T_{pre} \tag{6.46}$$

However, to control the trajectory from the computation of the desired roll angle ϕ_{des} an adaptation is needed. Instead of giving the information of a distance preview, a radius curvature preview R_{pre} could be a simple approach, by anticipating the curve with time.

$$R_c = R_{pre}(s_{pre}) \tag{6.47}$$

In equation 6.47, the radius curvature preview R_{pre} is defined in function of the reference line length preview s_{pre} for each time step. s_{pre} is computed by summing the actual reference line length s_t, in the time where the motorcycle is, and a length preview l_{pre}. The reference line length preview is given by:

$$s_{pre} = s_t + l_{pre} = s_t + v_x T_{pre} \tag{6.48}$$

Note that the l_{prev} differs form L_{prev}, where l_{prev} is a length in the reference line, as shown in Figure 6.20 and L_{prev} is a forward longitudinal distance from the motorcycle in order to found the target point in the reference line.

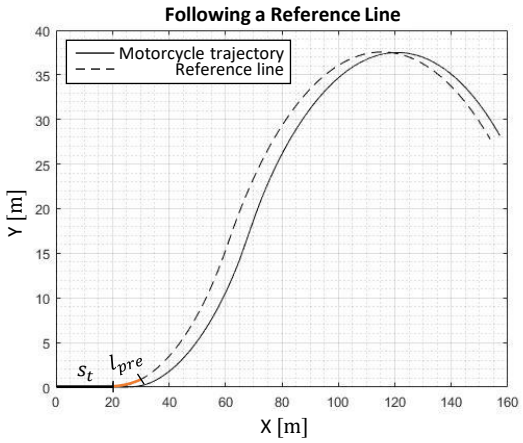

Figure 6.20: Representation of the actual reference line length s_t and length preview l_{pre} necessary for the strategy.

To implement the proposed method, following the preview distance strategy, it is necessary to account for the different delays caused by the intended lower or larger roll angles. The velocity of the motorcycle also affects the time necessary to reach the desired roll angle. Accomplished the relation between the time to achieved the desired roll angle, the radius of curvature preview R_{pre} can be finally calculated.

Chapter 7

Conclusions and Future Work

7.1 Conclusions

In this work, a motorcycle model of the TLM03e electric prototype was constructed for dynamic analysis, under different scenarios. It was presented the development of the contact detection and a track construction made by a mesh of triangles, enabling to represent with more detail the unevenness of the ground.

The implementation of a more realistic and specific tire model was challenging. The concept of a semi-empirical tire model reveals the necessity of a great amount of tire parameters database, making it very accurate when applied to the correct tire geometry. Unfortunately, in the literature, it was not possible to find the tire database for the tires used, leading to compute less realist forces and moments applied on the tires. Although, an easy and versatile implementation of the *Magic Formula* tire model is described.

The next objective of this work was the construction of the motorcycle multibody model of TLM03e prototype, allowing future studies of the prototype's dynamic aspects in more detail. In this phase it was evaluated the tire model, together with the motorcycle multibody model, in an unassisted scenario. As expected, the motorcycle model prescribed a straight line trajectory, accomplished mostly by the effect of the aligning moment and lateral forces applied.

Finally, the motorcycle dynamic behaviour was evaluated under the conditions of the controller. A simple reduced model is chosen to control the motorcycle over different scenarios. The simplified equations of motorcycle equilibrium for lateral, yawing, rolling and steering motion are derived. Therefore, to make use of a state vector with angular velocity in yaw axis and lateral velocity, the equations are already presented. Even though the simplified equations include a tire model, this is not consistent with the Pacejka tire model used in the motorcycle model. This difference between tire models, along with the imprecise tire model allocation on the motorcycle model, may reflect in a greater inefficiency of the controller in scenarios 2 and 3. Furthermore, better results could be achieved if the controller motorcycle parameters were updated at every time step, however more time for simulation would be needed. As stated in Chapter 6, the change of the coefficient $\mathbf{C}(4,1)$ is fundamental to motorcycle stability. A major

negative value of the coefficient results in less overshoot, but a greater error in the roll angle. If the coefficient becomes close to zero, stability problems can be found mainly for larger roll angles. Vehicle motion is also too sensitive to the matrices values of **Q** and **R**, being a relevant object of study for controller efficiency.

In an attempt to follow a reference line, a simplistic approach was implemented through the equation of steady state cornering. Instead of resorting to adding more state variables to handling the motorcycle over the reference line, the information was implicitly through the state variable roll angle ϕ. However, when scenario 4 is simulated, the motorcycle controller reveals the necessity of approaching the strategy of distance preview. An adaptation to the distance preview strategy was proposed in order to follow the reference line, where the radius of curvature information is re-evaluated based on the speed and position of the motorcycle to compute the desired roll angle ϕ_{des}.

7.2 Future Work

In an attempt to reproduce a more realist behaviour of a racing motorcycle in a track, the study of the rider dynamics around the motorcycle can be done in order to incorporate a multibody model of the pilot in the entire system modeled. Bench tests to the tire geometries used and for different tire compounds, can be financed to have a specific tire parameters database, ready to equip the motorcycle model and simulate in a racing track.

The vehicle motion is too sensitive to the coefficients prescribed for the matrices **Q**, **R** and **C**. A more reasonable selection of these coefficients is still an open question that needs to be addressed. The tracking of the motorcycle roll angle is highly dependent of these selections.

The velocity profile of the motorcycle along the track is a quantity that needs to be tracked in order to achieved a least time lap. The controller must be further developed to enforce that selected velocity profile, along the track, be achieved.

An investigation to the minimum time lap problem would be interesting. The idea of achieving a minimal time lap involves not only an optimal trajectory, with its corresponding optimal velocity profile, but also the tuning of the motorcycle setup. Motorcycle setup has a lot to do with its geometric parameters and suspension system. The strategy to develop track specific setups for the motorcycle is an open question for which optimization methods are promising tools.

Bibliography

[1] V. Cossalter. *Motorcycle Dynamics (Second Edition)*. 2006.

[2] Tony Foale. *Motorcycle Handling and Chassis Design*. 2002.

[3] P. E. Nikravesh. Computer Aided Analysis Mechanical Systems. 1988.

[4] Y. Shen, D. Xiang, X. Wang, L. Jiang, and Y. Wei. A contact force model considering constant external forces for impact analysis in multibody dynamics. *Multibody System Dynamics*, 44(4): 397–419, 2018.

[5] G. Gilardi and I. Sharf. Literature survey of contact dynamics modelling. *Mechanism and Machine Theory*, 37(10):1213–1239, 2002.

[6] G. Gim and P. E. Nikravesh. Analytical model of pneumatic tyres for vehicle dynamic simulations. Part 1. Pure slips. *International Journal of Vehicle Design*, 11(6):589–618, 1990.

[7] G. Gim and P. E. Nikravesh. Analytical model of pneumatic tyres for vehicle dynamic simulations. Part 2. Comprehensive slips. *International Journal of Vehicle Design*, 12(1):19–39, 1991. ISSN 01433369.

[8] G. Gim and P. E. Nikravesh. Analytical model of pneumatic tyres for vehicle dynamic simulations. Part 3. Validation against experimental data. *International Journal of Vehicle Design*, 12(2):217–228, 1991.

[9] H. B. Pacejka. *Tyre and Vehicle Dynamics*. Elsevier, 2nd edition, 2006.

[10] J. Baumgarte. Stabilization of constraints and integrals of motion in dynamical systems. *Computer Methods in Applied Mechanics and Engineering*, 1(1):1–16, 1972.

[11] R. Sharp, S. Evangelou, and D. Limebeer. Advances in the Modelling of Motorcycle Dynamics. *Multibody System Dynamics*, 12:251–283, 2004.

[12] R. Sharp. Stability, Control and Steering Responses of Motorcycles. *Vehicle System Dynamics*, 35:291–318, 2001.

[13] W. Langson and A. Alleyne. Multivariable bilinear vehicle control using steering and individual wheel torques. *Journal of Dynamic Systems, Measurement and Control, Transactions of the ASME*, 121 (4):631–637, 1999.

[14] P. Antos and J. A. C. Ambrósio. A Control Strategy for Vehicle Trajectory Tracking Using Multibody Models. *Multibody System Dynamics*, 11(4):365–394, 5 2004.

[15] Y. Marumo and M. Nagai. Steering control of motorcycles using steer-by-wire system. *User Modeling and User-Adapted Interaction*, 45(5):445–458, 2007.

[16] T. K. Dao and C. K. Chen. Path tracking control of a motorcycle based on system identification. *IEEE Transactions on Vehicular Technology*, 60(7):2927–2935, 2011.

[17] R. S. Sharp. The Stability And Control Of Motorcycles. *Vehicle System Dynamics*, 13(5):316–329, 1971.

[18] M. Yokomori, T. Oya, and A. Katayama. Rider control behavior to maintain stable upright position at low speed. *JSAE review*, 21(1):61–65, 2000.

[19] K. Huyge. Multibody Motorcycle , modelling and control. page 75, 2005.

[20] R. S. Sharp. Motorcycle steering control by road preview. *Journal of Dynamic Systems, Measurement and Control, Transactions of the ASME*, 129(4):373–381, 2007.

[21] J. Jaeger. Analytical solutions of contact impact problems. *Applied Mechanics Reviews*, 47(2): 35–54, 1994.

[22] J. J. Kalker. *Three-Dimensional Elastic Bodies in Rolling Contact*. 1990.

[23] G. Rill. Sophisticated but quite simple contact calculation for handling tire models. *Multibody System Dynamics*, 45(2):131–153, 2019.

Appendix A

Magic Formula for motorcycle

In the present appendix, will be presented all the equations necessary to compute the force and moment vectors to be applied to the tire. The equations are obtained from [9] and rewritten, making some simplifications and adaptations for the tire properties used.

The following parameters were defined with a small and equal value for all.

$$\varepsilon_x = \varepsilon_{Vx} = \varepsilon_y = \varepsilon_\gamma = \varepsilon_k = 0.001 \tag{A.1}$$

To calculate $\cos' \alpha$, the small quantity ε_{Vx} is taking into account. Taking advantage of expression 4.15 follows:

$$\cos' \alpha = \cos\left\{\arctan\left(\frac{V_{Sy}}{\max[V_{Cx}, \varepsilon_{Vx}]}\right)\right\} \tag{A.2}$$

A.1 Pure Slip

A.1.1 Longitudinal Force, F_{x0}

$$K_{x\kappa} = F_z \cdot (p_{Kx1} + p_{Kx2} df_z) \cdot \exp(p_{Kx3} df_z) \tag{A.3}$$

$$S_{Vx} = F_z \cdot (p_{Vx1} + p_{Vx2} df_z) \cdot \{|V_{Cx}|/(\varepsilon_{Vx} + |V_{Cx}|)\} \tag{A.4}$$

$$S_{Hx} = -(q_{Sy1} F_z + S_{Vx})/K_{x\kappa} \tag{A.5}$$

$$\kappa_x = \kappa + S_{Hx} \tag{A.6}$$

$$D_x = (p_{Dx1} + p_{Dx2} df_z) \cdot F_z \qquad (> 0) \tag{A.7}$$

$$E_x = (p_{Ex1} + p_{Dx2} df_z + p_{Dx3} df_z^2) \cdot \{1 - p_{Ex4} sgn(\kappa_x)\} \qquad (\leq 1) \tag{A.8}$$

$$B_x = K_{x\kappa}/(C_x D_x + \varepsilon_x) \tag{A.9}$$

$$F_{x0} = D_x \sin[C_x \arctan\{B_x\kappa_x - E_x(B_x\kappa_x - \arctan(B_x\kappa_x))\}] + S_{Vx} \tag{A.10}$$

A.1.2 Lateral Force, F_{y0}

$$S_{Hy} = p_{Hy1} \tag{A.11}$$

$$\alpha_y = \alpha^* + S_{Hy} \tag{A.12}$$

$$C_y = p_{Cy1} \qquad (> 0) \tag{A.13}$$

$$D_y = \left\{p_{Dy1} \cdot \exp(p_{Dy1} df_z)/(1 + p_{Dy3}\gamma^2)\right\} \cdot F_z \qquad (> 0) \tag{A.14}$$

$$E_y = p_{Ey1} + p_{Dy2}\gamma^2 + (p_{Ey3} + p_{Ey4}\gamma) sgn(\alpha_y) \qquad (\leq 1) \tag{A.15}$$

$$K_{y\alpha 0} = p_{Ky1} F_{z0} \sin\left[p_{Ky2} \arctan\left\{F_z/((p_{Ky3} + p_{Ky4}\gamma^2)F_{z0})\right\}\right] \tag{A.16}$$

$$K_{y\alpha} = K_{y\alpha 0}/(1 + p_{Ky5}\gamma^2) \tag{A.17}$$

$$B_y = K_{y\alpha}/(C_y D_y + \varepsilon_y) \tag{A.18}$$

$$C_\gamma = p_{Cy2} \qquad (> 0) \tag{A.19}$$

$$E_\gamma = p_{Ey5} \qquad (\leq 1) \tag{A.20}$$

$$K_{y\gamma} = (p_{Ky6} + p_{Ky7} df_z) \cdot F_z \tag{A.21}$$

$$B_\gamma = K_{y\gamma}/(C_\gamma D_y + \varepsilon_y) \tag{A.22}$$

$$\begin{aligned} F_{y0} = D_y \sin\big[C_y \arctan\left\{B_y\alpha_y - E_y(B_y\alpha_y - \arctan(B_y\alpha_y))\right\} + \\ + C_\gamma \arctan\left\{B_\gamma\gamma - E_\gamma(B_\gamma\gamma - \arctan(B_\gamma\gamma))\right\}\big] \qquad (C_y + C_\gamma < 2) \end{aligned} \tag{A.23}$$

A.1.3 Aligning Moment, M_{z0}

$$\alpha_t = \alpha^* \tag{A.24}$$

$$C_t = q_{Cz1} \qquad (> 0) \tag{A.25}$$

$$B_t = (q_{Bz1} + q_{Bz2} df_z + q_{Bz3} df_z^2) \cdot (1 + q_{Bz5}|\gamma| + q_{Bz6}\gamma^2) \qquad (> 0) \tag{A.26}$$

$$D_t = F_z \cdot (R_0/F_{z0}) \cdot (q_{Dz1} + q_{Dz2} df_z) \cdot (1 + q_{Dz3}|\gamma| + q_{Dz4}\gamma^2) \tag{A.27}$$

$$E_t = (q_{Ez1} + q_{Ez2} df_z + q_{Ez3} df_z^2) \cdot \left\{1 + (q_{Ez4} + q_{Ez5}\gamma)\frac{2}{\pi}\arctan(B_t C_t \alpha_t)\right\} \qquad (\leq 1) \tag{A.28}$$

$$M_{zt0} = -D_t \cos\left[C_t \arctan\left\{B_t\alpha_t - E_t(B_t\alpha_t - \arctan(B_t\alpha_t))\right\}\right] \cdot \cos'\alpha \cdot F_{y0,\gamma=0} \tag{A.29}$$

$$S_{Hr} = q_{Hz1} + q_{Hz2} df_z + (q_{Hz3} + q_{Hz4} df_z)\gamma \tag{A.30}$$

$$\alpha_r = \alpha^* + S_{Hr} \tag{A.31}$$

$$B_r = q_{Bz9} + q_{Bz10} B_y C_y \tag{A.32}$$

$$D_r = F_z R_0 \left\{(q_{Dz6} + q_{Dz7} df_z) + (q_{Dz8} + q_{Dz9} df_z)\gamma + (q_{Dz10} + q_{Dz11} df_z)\gamma|\gamma|\right\} \cdot \cos'\alpha \tag{A.33}$$

$$M_{zr0} = D_r \cos\left[\arctan(B_r\alpha_r)\right] \tag{A.34}$$

$$M_{z0} = M_{zt0} + M_{zr0} \tag{A.35}$$

A.2 Combined Slip

A.2.1 Longitudinal Force, F_x

$$S_{Hx\alpha} = r_{Hx1} \tag{A.36}$$

$$\alpha_S = \alpha^* + S_{Hx\alpha} \tag{A.37}$$

$$C_{x\alpha} = r_{Cx1} \tag{A.38}$$

$$B_{x\alpha} = (r_{Bx1} + r_{Bx3}\gamma^2)\cos\left[\arctan(r_{Bx2}\kappa)\right] \qquad (> 0) \tag{A.39}$$

$$G_{x\alpha 0} = \cos\left[C_{x\alpha}\arctan(B_{x\alpha}S_{Hx\alpha})\right] \tag{A.40}$$

$$G_{x\alpha} = \cos\left[C_{x\alpha}\arctan(B_{x\alpha}\alpha_S)\right]/G_{x\alpha 0} \qquad (> 0) \tag{A.41}$$

$$F_x = G_{x\alpha}\cdot F_{x0} \tag{A.42}$$

A.2.2 Lateral Force, F_y

$$S_{Hy\kappa} = r_{Hy1} + r_{Hy2}df_z \tag{A.43}$$

$$\kappa_S = \kappa + S_{Hy\kappa} \tag{A.44}$$

$$C_{y\kappa} = r_{Cy1} \tag{A.45}$$

$$B_{y\kappa} = (r_{By1} + r_{By4}\gamma^2)\cos\left[\arctan\left\{r_{By2}(\alpha^* - r_{By3})\right\}\right] \qquad (> 0) \tag{A.46}$$

$$G_{y\kappa 0} = \cos\left[C_{y\kappa}\arctan(B_{y\kappa}S_{Hy\kappa})\right] \tag{A.47}$$

$$G_{y\kappa} = \cos\left[C_{y\kappa}\arctan(B_{y\kappa}\kappa_S)\right]/G_{y\kappa 0} \qquad (> 0) \tag{A.48}$$

$$D_{Vy\kappa} = D_y\cdot(r_{Vy1} + r_{Vy2}df_z + r_{Vy3}\gamma)\cdot\cos\left[\arctan(r_{Vy4}\alpha^*)\right] \tag{A.49}$$

$$S_{Vy\kappa} = D_{Vy\kappa}\sin\left[r_{Vy5}\arctan(r_{Vy6}\kappa)\right] \tag{A.50}$$

$$F_y = G_{y\kappa}\cdot F_{y0} + S_{Vy\kappa} \tag{A.51}$$

A.2.3 Overturning Couple, M_x

$$M_x = F_z R_0\cdot(q_{sx1} - q_{sx2}\gamma + q_{sx3}F_y/F_{z0}) \tag{A.52}$$

A.2.4 Rolling Resistance Moment, M_y

$$M_y = -F_z R_0\cdot(q_{sy1} + q_{sy2}F_x/F_{z0}) \tag{A.53}$$

A.2.5 Aligning Torque, M_z

$$\alpha_{t,eq} = \sqrt{\alpha_t^2 + \left(\frac{K_{y\kappa}}{K_{y\alpha} + \varepsilon_k}\right)^2 \kappa^2} \cdot sgn(\alpha_t) \tag{A.54}$$

$$\alpha_{r,eq} = \sqrt{\alpha_r^2 + \left(\frac{K_{y\kappa}}{K_{y\alpha} + \varepsilon_k}\right)^2 \kappa^2} \cdot sgn(\alpha_r) \tag{A.55}$$

$$F_{y,\gamma=0} = G_{y\kappa} \cdot F_{y0,\gamma=0} \tag{A.56}$$

$$F'_y = F_{y,\gamma=0} - S_{V y\kappa} \tag{A.57}$$

$$M_{zr} = D_r \cos\left[\arctan(B_r \alpha_{r,eq})\right] \tag{A.58}$$

$$M_{zt} = -D_t \cos\left[C_t \arctan\left\{B_t \alpha_{t,eq} - E_t(B_t \alpha_{t,eq} - \arctan(B_t \alpha_{t,eq}))\right\}\right] \cdot \cos' \alpha \cdot F'_y \tag{A.59}$$

$$s = R_0 \cdot \left\{s_{sz1} + s_{sz2}(F_y/F_{z0}) + (s_{sz3} + s_{sz4} df_z)\gamma\right\} \tag{A.60}$$

$$M_z = M_{zt} + M_{zr} + s \cdot F_x \tag{A.61}$$

Appendix B

Tire Properties

Table B.1: Tire properties used for the Pacejka model applied to the front and rear tires.

Vertical	C_z = 200000	D_z = 50	F_{z0} = 1200	D_{reff} = 0.27
	B_{reff} = 8.4	F_{reff} = 0.07		
Longitudinal	p_{Cx1} = 1.7655	p_{Dx1} = 1.2839	p_{Dx2} = −0.0078226	p_{Ex1} = 0.4743
	p_{Ex2} = 9.387e−05	p_{Ex3} = 0.066154	p_{Ex4} = 0.00011999	p_{Kx1} = 25.383
	p_{Kx2} = 1.0978	p_{Kx3} = 0.19775	p_{Vx1} = 2.167e−05	p_{Vx2} = 4.746e−05
	r_{Bx1} = 12.084	r_{Bx2} = −8.3959	r_{Bx3} = 2.197e−09	r_{Cx1} = 1.0648
	r_{Hx1} = 0.0			
Lateral	p_{Cy1} = 1.1086	p_{Cy2} = 0.66464	p_{Dy1} = 1.3898	p_{Dy2} = −0.0044718
	p_{Dy3} = 0.21428	p_{Ey1} = −0.80276	p_{Ey2} = 0.89416	p_{Ey3} = 0.0
	p_{Ey4} = 0.0	p_{Ey5} = −2.8159	p_{Ky1} = −19.747	p_{Ky2} = 1.3756
	p_{Ky3} = 1.3528	p_{Ky4} = −1.2481	p_{Ky5} = 0.3743	p_{Ky6} = −0.91343
	p_{Ky7} = 0.2907	p_{Hy1} = 0.0	r_{By1} = 10.694	r_{By2} = 8.9413
	r_{By3} = 0.0	r_{By4} = −1.826e−10	r_{Cy1} = 1.0521	r_{Hy1} = −7.864e−05
	r_{Hy2} = −6.900e−05	r_{Vy1} = 0.0	r_{Vy2} = 0.0	r_{Vy3} = −0.00033208
	r_{Vy4} = −4.791e−15	r_{Vy5} = 1.9	r_{Vy6} = −30.082	
Aligning	q_{Bz1} = 9.246	q_{Bz2} = −1.4442	q_{Bz3} = −1.8323	q_{Bz5} = 0.15703
	q_{Bz6} = 0.0	q_{Bz9} = 8.3146	q_{Bz10} = 0.0	q_{Cz1} = 1.2813
	q_{Dz1} = 0.063288	q_{Dz2} = −0.015642	q_{Dz3} = −0.060347	q_{Dz4} = −0.45022
	q_{Dz6} = 0.0	q_{Dz7} = 0.0	q_{Dz8} = −0.08525	q_{Dz9} = −0.081035
	q_{Dz10} = 0.030766	q_{Dz11} = 0.074309	q_{Ez1} = −3.261	q_{Ez2} = 0.63036
	q_{Ez3} = 0.0	q_{Ez4} = 0.0	q_{Ez5} = 0.0	q_{Hz1} = 0.0
	q_{Hz2} = 0.0	q_{Hz3} = 0.0	q_{Hz4} = 0.0	s_{sz1} = 0.0
	s_{sz2} = 0.0033657	s_{sz3} = 0.16833	s_{sz4} = 0.017856	
Overturning	q_{sx1} = 0.0	q_{sx2} = 0.16056	q_{sx3} = 0.095298	
Rolling	q_{sy1} = 0.01	q_{sy2} = 0.0		

Appendix C

Controller Tire Properties

Next expressions of tire forces and moments, were taken from [15] to be used on the simplified equation of motorcycle equilibrium:

$$Y_f = -C_{YS1}\alpha_f + C_{YC1}\phi_f$$

$$Y_r = -C_{YS2}\alpha_r + C_{YC2}\phi_r$$

$$T_{xf} = -C_{XS1}\alpha_f + C_{XC1}\phi_f$$

$$T_{xr} = -C_{XS2}\alpha_r + C_{XC2}\phi_r$$

$$T_{zf} = -C_{ZS1}\alpha_f + C_{ZC1}\phi_f$$

$$T_{zr} = -C_{ZS2}\alpha_r + C_{ZC2}\phi_r \; \alpha_f = (\dot{y}_1 + l_1\dot{\psi} - t\dot{\delta})\frac{1}{v} - \delta\cos\tau$$

$$\alpha_r = (\dot{y}_1 - l_2\dot{\psi})\frac{1}{v}$$

$$\phi_f = \phi + \delta\cos\tau$$

$$\phi_r = \phi$$

The tire parameters are described in linear functions of the tire vertical load, being expressed as $C = C_1|Z_{f,r}| + C_2 = (C_1, C_2)$, where $Z_{f,r}$ means the vertical load.

$$C_{YS1} = (9.12, 3480)[N/rad]$$

$$C_{YS2} = (4.87, 4440)[N/rad]$$

$$C_{YC1} = (1.43, -275)[N/rad]$$

$$C_{YC2} = (1.16, 73.0)[N/rad]$$

$$C_{ZS1} = (0.244, -106)[Nm/rad]$$

$$C_{ZS2} = (0.208, -139)[Nm/rad]$$

$$C_{ZC1} = (0.0140, -6.12)[Nm/rad]$$

$$C_{ZC2} = (0.0147, -1.68)[Nm/rad]$$

$$C_{XS1} = (0.180, -138)[Nm/rad]$$

$$C_{XS2} = (0.159, -173)[Nm/rad]$$

$$C_{XC1} = (0.0688, -14.6)[Nm/rad]$$

$$C_{XC2} = (0.0900, -33.7)[Nm/rad]$$